An Energy Framework to Control Viscoelastic SemiActive Devices in PlanWise OneWay Asymmetric Systems

Wiley
Structural Control and Health Monitoring
Volume 2025, Article ID 7091316, 34 pages
https://doi.org/10.1155/stc/7091316

WILEY

Research Article

An Energy Framework to Control Viscoelastic Semi-Active Devices in Plan-Wise One-Way Asymmetric Systems

M. De Iuliis, E. Miceli, and P. Castaldo

Department of Structural, Geotechnical and Building Engineering (DISEG), Politecnico di Torino, Corso Duca degli Abruzzi 24, Turin 10129, Italy

Correspondence should be addressed to M. De Iuliis; massimiliano.deiuliis@polito.it

Received 15 November 2024; Accepted 11 March 2025

Academic Editor: Yoshiki Ikeda

This study proposes new strategies for the semi-active control of the dynamic response of a plan-wise asymmetrical structural system using viscoelastic devices. Different from some literature proposals, these innovative strategies are designed to be immediately interpretable, aiming to optimize the different terms of the energy balance equation through a set of closed-form analytical control algorithms to manage the properties of semi-active devices. Specifically, four algorithms have been developed to maximize the energy dissipated by the system or minimize the elastic energy, kinetic energy, and input energy. These algorithms have been tested through an extensive numerical investigation by modifying the main structural parameters of the asymmetrical system and considering 85 accelerometric input signals with different dynamic characteristics related to both far-field and near-fault records. The effectiveness of the four proposed strategies, aimed to modify the semi-active device properties, was evaluated by comparing the seismic responses of asymmetric systems, in terms of both relative displacement and energy components, with the regular configuration of semi-active devices (i.e., passive control) and other algorithms, such as "Kamagata & Kobori" and "sky hook" finalized, respectively, to manage stiffness and damping extra-structural resources. The results demonstrated the effectiveness of the proposed strategies, especially, in the presence of flexible systems and high-demanding near-fault seismic events.

Keywords: asymmetric system; energy balance; far-field and near-fault seismic events; semi-active devices; structural control; viscoelastic damping

1. Introduction

As supported by theoretical and experimental scientific evidence, it is well-established that the effects of high-intensity seismic events are markedly greater in structural systems with non-uniform distribution of both mass and stiffness (i.e., asymmetric structures). Therefore, these systems should be considered more vulnerable to seismic actions compared to regular structural systems [1, 2]. A detailed analysis of the damage caused by the Mexico City earthquake (1985) [3] highlighted that a large portion of the collapsed structures had significant irregularities in the distribution of strength and stiffness, both vertically and plan-wise. Similarly, during the Kocaeli earthquake, on November 12, 1999, some structures were severely damaged due to partial retrofitting interventions carried out to repair minor damages after the earthquake on August 17 of the same year, which significantly increased the level of asymmetry in the distribution of stiffness [4]. Even in recent events, such as the earthquake in Turkey and Syria on February 6, 2023, several buildings suffered substantial damages due to reinforcement operations that were conceived without considering, adequately, their effect on stiffness distribution and consequential activation of large torsional moments [5]. Base-isolated buildings also appear to be more vulnerable when characterized by significant asymmetry, as demonstrated by a specific study conducted on the dynamic response of an asymmetric L-shaped structure, a 7-story and 14-story building, to the Tohoku Earthquake (2011) [6].

The dynamic response of plan-asymmetric systems still presents significant issues, which can be summarized, though not exhaustively, as follows: (i) complexity in identifying and measuring the level of irregularity due to asymmetry, (ii) difficulty in selecting analysis and design methods, in both linear and nonlinear fields, to obtain a reliable estimate of the seismic demand [7].

For several years, these systems have been investigated to evaluate the effectiveness of different design strategies aimed at mitigating the lateral–torsional response [8–10]. More recently, two new research areas have been developed: the study of seismic response using nonlinear static methods together with their reliability [11–17] and the use of control devices to balance the seismic demand in the different components of the structural system. The latter research area has developed rapidly, providing very promising results in terms of practical applications, both for the high-performance levels that can be achieved and for the increasingly advanced technological developments.

In fact, various types of semi-active devices with controllable properties have been investigated. In viscous actuators, a fluid is used to dissipate motion energy, and damping is achieved through the relative velocity between the different parts of the device. In viscoelastic devices, the operating mechanism generally involves materials that deform reversibly under load, offering both variable damping and stiffness [18–23]. Frictional devices typically involve surfaces in relative motion, dissipating energy by rubbing against each other in proportion to the applied pressure. These devices are particularly reliable but have the drawback of being noisy and generating heat during operations [24, 25].

X-plate dampers [26, 27], on the other hand, offer an alternative passive energy dissipation mechanism that relies on the controlled plastic deformation of steel plates, effectively mitigating vibrations without the issues associated with friction-based systems. Their optimized design allows for efficient lateral–torsional control while maintaining durability and low maintenance requirements. Tuned mass dampers (TMDs) use an additional mass connected to the main structure through elastic elements and dampers. This mass is designed to oscillate at the resonance frequency of the structure, thereby reducing vibrations. A variant of this concept is represented by tuned liquid dampers, in which the liquid in a tank oscillates in response to the vibrations of the structure [28–34] as well as tuned mass friction dampers (TMFDs), which consist of a TMD with linear stiffness and pure friction damper leading to a nonlinear behavior [35–37]. The dynamic characteristics of a TMD can be semi-actively controlled to enhance its performance. In this context, Sun and Nagarajaiah [38] have shown that a semiactive TMD (STMD) with variable damping ratio and frequency can effectively attenuate seismic responses and outperform the optimal passive TMD. Wang et al. [39] developed an adaptive-passive variable pendulum TMD (APVP-TMD) identifying the optimal TMD frequency through wavelet transformation by an acceleration sensor and a microcontroller; its effectiveness was proved for both discrete and continuous models.

Moreover, combined strategies are also considered. Seismic performance of base-isolated structures can be significantly enhanced by integrating an STMD, which achieves high control performance in both linear and nonlinear models by effectively mitigating the structural first-mode response and reducing dynamic responses at both the top story and the isolated level, as demonstrated in Wang et al. [40]. Karami and Ahmadi [41] attempted to reduce the torsional effects and dynamic responses of the structure by combining two strategies: real-time structural health monitoring and semi-active control.

Within semi-active devices, magnetorheological (MR) devices play a significant role: they use fluids whose viscosity changes in response to an applied magnetic field. This allows for a rapid and controlled variation of the damping level. These actuators are very versatile and have the advantage of becoming passive devices in case of failure [42–47].

Despite the substantial research efforts dedicated to seismic mitigation strategies, the dynamic response of asymmetric structures remains an unresolved challenge. In fact, most studies on semi-active control systems primarily address the translational response, with a significantly lower focus on the coupled torsional response. This represents a critical limitation, as real structures often exhibit strong interactions between lateral and torsional motion, which can amplify seismic demand and increase structural vulnerability. Furthermore, existing numerical models frequently fail to accurately capture the combined effects of energy dissipation and latero-torsional coupling in semi-active controlled asymmetric systems, thereby constraining the predictive value of current analytical methodologies.

Regarding the algorithms designed to manage semi-active devices, several studies have been proposed in the literature to enhance the seismic performance of asymmetric structural systems. The first significant contribution for electrorheological devices is by McClamroch and Gavin [48], who proposed a control law that explicitly takes into account their nonlinear behavior and, by using a Lyapunov-based control synthesis, leads to a "bang-bang" control rule, which minimizes the energy from the seismic signal transmitted to the structure. This strategy is particularly efficient in attenuating the peak seismic response during the first few seconds of an event. Later, Dyke et al. [49] proposed a clipped-optimal control strategy based on acceleration feedback to control MR dampers, with the aim of reducing structural seismic responses. Results show that the semi-active control system is capable of not only approaching but surpassing the performance of a linear active control system while requiring only a small fraction of the power needed by the active controller. Sadek & Mohraz [50] compared the effectiveness of three algorithms in mitigating the seismic response of plan-wise asymmetrical systems through semi-active devices: a linear quadratic regulator, a generalized

quadratic regulator with acceleration penalization, and a displacement-acceleration domain algorithm. Meanwhile, Li and Gu [32] proposed to simulate the optimal control action obtained using an LQR (Linear Quadratic Riccati) algorithm with a minimum norm method (MNM) through passive viscous devices, achieving promising results. Pnevmatikos and Hatzigeorgiou [51] proposed a control algorithm applicable to both active and semi-active devices based on pole placement. The procedure is based on creating a fictitious symmetrical structure to calculate and apply suitable poles improving, significantly, seismic behavior with minimal control forces. Sever et al. [52] presented an optimal control algorithm based on linear matrix inequalities (LMIs). Numerical simulations showed that the controller effectively reduces vibrations and ensures stability of asymmetrical systems, improving both frequency and time-domain responses.

These algorithms are effective in reducing translational response but are not specifically tailored to address torsional effects in asymmetric buildings; moreover, they lack a clear physical interpretation, which prevents a full understanding of their effectiveness and robustness. One possible interpretative key is based on the concept of energy and energy balance, a perspective introduced by Goel [53] in the context of the seismic response of asymmetric systems and, more generally, by Yanik et al. [54] in the field of structural control. Few contributions in the literature address algorithms based on direct energy control (e.g., [55]). The same authors have proposed an approach based on optimizing different energy components, specifically, for viscous devices [56].

This study proposes to generalize the energetic approach to semi-active devices, arranged within an asymmetric structural system, capable of modifying both their damping and stiffness properties. Indeed, four strategies are proposed to control the torsional response of asymmetric systems using semi-active devices generally allocated throughout the structure and capable of modifying both the damping and stiffness in real time. Such strategies are based on the optimization of energy terms: dissipated energy, kinetic energy, elastic energy, and input energy, evaluated by directly considering the dynamics of the asymmetric system. This approach offers the advantage of explicitly accounting for the mechanical properties of the system to be protected while also being fully interpretable from a physical perspective.

This manuscript is organized as follows: in Section 2, the dynamic issue of an asymmetrical one-way plan-wise system equipped with viscoelastic devices is presented, and its energy balance is studied. In Section 3, the individual energy terms are analyzed to identify, in closed form, the control algorithms for the dynamic response based on energy optimization over time. In the other sections, assuming a fixed regular configuration of the semi-active devices, these control algorithms are tested considering several asymmetrical plan-wise systems, with properties of engineering interest, and several input excitations with different characteristics related to both far-field and near-fault records [57]. The results obtained in reducing the seismic response are compared with those achievable through passive system control and well-known and reliable algorithms, such as "Kamagata & Kobori" and "sky hook," finalized, respectively, to manage stiffness and damping extra-structural resources. The results, in terms of both relative displacement and energy components, demonstrated the effectiveness of the proposed strategies, especially, in the case of flexible systems and high-demanding near-fault seismic events.

2. Dynamic Issue for an Asymmetrical One-Way System

Let us consider the structural system represented in Figure 1, whose dynamics is described with respect to the x–y coordinate system, with the origin at the center of mass (O_M) and the x-axis direction coinciding with the line connecting the center of mass (O_M) with the center of stiffness (O_k). The system is one-way, assuming that the available damping and stiffness additional resources are placed along the y direction. This assumption is consistent with the objective of reducing torsional effects without introducing an additional component of eccentricity into the system.

The structural system is characterized by its mass, M, the rotational inertia of the mass around its center, I_θ, and the corresponding radius of gyration, ρ_M. The asymmetry of the structural system, in its original configuration without control devices, is defined by the eccentricity, e_{kx}, that is, the distance between the center of mass and the center of stiffness, as well as by the radius of gyration of the stiffness distribution with respect to the O_k point, ρ_k. Furthermore, an intrinsic Rayleigh damping will be considered for the system, whose coefficients α and β can be evaluated to obtain a preassigned level of inherent damping factor on the first two modes of the system.

The presence of extra-structural viscoelastic semi-active devices can be described by four parameters: the position of the supplementary damping center (O_{CD}), whose x-coordinate is indicated as e_{Cx}, its radius of gyration with respect to a vertical axis passing through O_{CD}, ρ_{CD}, the position of the supplementary stiffness center (O_{KD}), whose x-coordinate is denoted as e_{Kx}, and its radius of gyration with respect to a vertical axis passing through the O_{KD}, ρ_{KD}. It follows that an extra-structural stiffness resource modifies the overall asymmetry properties of the system, directly affecting the overall eccentricity of the system and the radius of gyration.

The dynamic parameters of the system equipped with viscoelastic semi-active devices are defined as a function of both the value and position of the stiffness and damping elements, as follows:

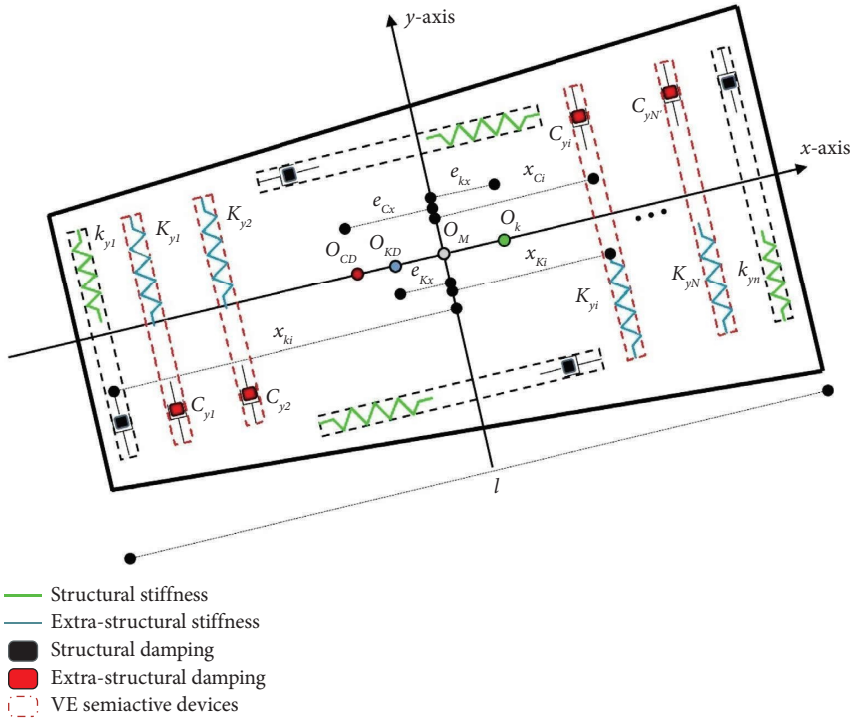

FIGURE 1: Asymmetrical plan-wise system equipped with viscoelastic semi-active devices.

$$k_y = \sum_{i=1}^{n} k_{yi} \text{ overall structural stiffness,} \tag{1a}$$

$$K_y = \sum_{i=1}^{N} K_{yi} \text{ overall extra-structural stiffness,} \tag{1b}$$

$$C_y = \sum_{i=1}^{N'} C_{yi} \text{ overall extra-structural damping,} \tag{1c}$$

$$e_{\mathrm{kx}} = \frac{1}{k_y} \sum_{i=1}^{n} k_{yi} \cdot x_{ki} \text{ structural eccentricity,} \tag{1d}$$

$$e_{\mathrm{Kx}} = \frac{1}{K_y} \cdot \sum_{i=1}^{N} K_{yi} \cdot x_{Ki} \text{ extra-structural stiffness eccentricity,} \tag{1e}$$

$$e_{Cx} = \frac{1}{C_y} \cdot \sum_{i=1}^{N'} C_{yi} \cdot x_{Ci} \text{ extra-structural damping eccentricity,} \tag{1f}$$

$$k_\theta = \sum_{i=1}^{n} k_{yi} \cdot x_{ki}^2 = k_y \cdot e_{kx}^2 + k_{\theta R} \text{ structural torsional stiffness,} \tag{1g}$$

$$K_\theta = \sum_{i=1}^{N} K_{yi} \cdot x_{Ki}^2 = K_y \cdot e_{Kx}^2 + K_{\theta R} \text{ extra-structural torsional stiffness,} \tag{1h}$$

$$C_\theta = \sum_{i=1}^{N'} C_{yi} \cdot x_{Ci}^2 = C_y \cdot e_{Cx}^2 + C_{\theta R} \text{ extra-structural torsional damping,} \tag{1i}$$

$$\rho_M = \sqrt{\frac{I_\theta}{M}} \text{ mass radius of gyration,} \tag{1l}$$

$$\rho_k = \sqrt{\frac{k_{\theta R}}{k_y}} \text{ structural stiffness radius of gyration,} \tag{1m}$$

$$\rho_{\mathrm{KD}} = \sqrt{\frac{K_{\theta R}}{K_y}} \text{ extra-structural stiffness radius of gyration,} \tag{1n}$$

$$\rho_{\mathrm{CD}} = \sqrt{\frac{C_{\theta R}}{C_y}} \text{ extra-structural damping radius of gyration,} \tag{1o}$$

where k_{yi} represents the lateral stiffness of the i-th resistant element, K_{yi} is the lateral stiffness of the i-th extra-structural resistant element, C_{yi} is the damping coefficient of the i-th extra-structural dissipative element, x_{ki} is the distance from O_M of the i-th resistant element along the x-axis, x_{Ki} is the distance from O_M of the i-th extra-structural resistant element along the x-axis, x_{Ci} is the distance from O_M of the i-th extra-structural dissipative element along the x-axis, $k_{\theta R}$ is the torsional stiffness of the structural system with respect to a vertical axis passing through O_k, $K_{\theta R}$ is the extra-structural torsional stiffness with respect to a vertical axis passing through O_{KD}, and $C_{\theta R}$ is the extra-structural torsional damping coefficient with respect to a vertical axis passing through O_{CD}. Note that for easier reading and interpretation of the stiffness terms, lowercase letters are used for structural quantities, whereas uppercase letters are used for terms related to viscoelastic devices (i.e., extra-structural elements).

The equations of motion governing the dynamics of the system subject to a seismic input signal $\ddot{u}_g$, in which the two degrees of freedom represent the displacement of the center of mass along the y direction and the rotation of the deck around a vertical axis passing through the center of mass, θ, can be written, considering a Rayleigh damping, in a dimensional form as follows:

$$M\ddot{y} + \left(\alpha M + \beta k_y\right)\dot{y} + \beta k_y e_{kx}\dot{\theta} + C_y\dot{y} + C_y e_{Cx}\dot{\theta} + k_y y + k_y e_{kx}\theta + K_y y + K_y e_{Kx}\theta = -M\ddot{u}_g, \tag{2}$$

$$\begin{aligned} &I_M\ddot{\theta} + \beta k_y e_{kx}\dot{y} + \left(\alpha I_M + \beta k_y e_{kx}^2 + \beta k_{\theta R}\right)\dot{\theta} + C_y e_{Cx}\dot{y} + C_y e_{Cx}^2\dot{\theta} \\ &\quad + C_{\theta R}\dot{\theta} + k_y e_{kx} y + k_y e_{kx}^2\theta + k_{\theta R}\theta + K_y e_{Kx} y + K_y e_{Kx}^2\theta + K_{\theta R}\theta = 0. \end{aligned} \tag{3}$$

Dividing Equation (2) by M and Equation (3) by $M \cdot l$, Equations (2) and (3) become dimensionally homogeneous, as follows:

$$\ddot{y} + \left(\alpha + \beta\omega_y^2\right)\dot{y} + \beta\omega_y^2\varepsilon_{kx}\dot{\theta}l + 2\omega_y\xi_y\dot{y} + 2\omega_y\xi_y\varepsilon_{Cx}\dot{\theta}l + \omega_y^2 y + \omega_y^2\varepsilon_{kx}\theta l + \omega_y^2 r_K y + \omega_y^2 r_K\varepsilon_{Kx}\theta l = -\ddot{u}_g, \tag{4}$$

$$\begin{aligned} &\lambda_M^2\ddot{\theta}l + \beta\omega_y^2\varepsilon_{kx}\dot{y} + \left(\alpha\lambda_M^2 + \beta\omega_y^2\varepsilon_{kx}^2 + \beta\lambda_k^2\right)\dot{\theta}l + 2\omega_y\xi_y\varepsilon_{Cx}\dot{y} + 2\omega_y\xi_y\varepsilon_{Cx}^2\dot{\theta}l + \lambda_C^2\dot{\theta}l + \omega_y^2\varepsilon_{kx} y + \omega_y^2\varepsilon_{kx}^2\theta l \\ &\quad + \lambda_k^2\theta l + \omega_y^2 r_K\varepsilon_{Kx} y + \omega_y^2 r_K\varepsilon_{Kx}^2\theta l + \lambda_K^2\theta l = 0, \end{aligned} \tag{5}$$

where the following parameters are defined:

- l characteristic length of the system in the x direction;
- y, θ relative translational and rotational displacement;
- $\omega_y = \sqrt{k_y/M}$ natural circular frequency of the system's translational motion in the y direction;
- $\varepsilon_{kx} = e_{kx}/l$ non-dimensional structural eccentricity;

- $r_K = K_y/k_y$ ratio between extra-structural and structural stiffness in the y direction;
- $\varepsilon_{Kx} = e_{Kx}/l$ non-dimensional eccentricity of extra-structural stiffness;
- $\xi_y = C_y/(2M\omega_y)$ equivalent extra-structural damping coefficient;
- $\varepsilon_{Cx} = e_{Cx}/l$ non-dimensional eccentricity of extra-structural damping;
- $\lambda_M = \rho_M/l = (1/l)\sqrt{I_\theta/M}$ non-dimensional mass radius of gyration;
- $\lambda_k = \rho_k/l = (1/l)\sqrt{k_{\theta R}/k_y}$ non-dimensional structural stiffness radius of gyration;
- $\lambda_K = \rho_{KD}/l = (1/l)\sqrt{K_{\theta R}/K_y}$ non-dimensional extra-structural stiffness radius of gyration;
- $\lambda_C = \rho_{CD}/l = (1/l)\sqrt{C_{\theta R}/C_y}$ non-dimensional extra-structural damping radius of gyration.

The coefficients α and β are evaluated by solving the following system of equations:

$$\begin{cases} \dfrac{\alpha}{\omega_1} + \beta\omega_1 = 2\xi_1, \\ \dfrac{\alpha}{\omega_2} + \beta\omega_2 = 2\xi_2, \end{cases} \tag{6}$$

in which ω_1 and ω_2 represent the circular frequencies of the two modes and depend on the dynamic properties of the system. In the following numerical analysis, the intrinsic damping factors on the first two modes $\xi_1 = \xi_2$ will be considered equal to 0.02.

Equations (4) and (5) can be combined with the abovementioned parameters into a matrix form, as follows:

$$\begin{bmatrix} 1 & 0 \\ 0 & \lambda_M^2 \end{bmatrix}\begin{bmatrix} \ddot{y} \\ \ddot{\theta} l \end{bmatrix} + \left(\alpha\begin{bmatrix} 1 & 0 \\ 0 & \lambda_M^2 \end{bmatrix} + \beta\omega_y^2\begin{bmatrix} 1 & \varepsilon_{kx} \\ \varepsilon_{kx} & \varepsilon_{kx}^2 + \lambda_k^2 \end{bmatrix}\right)\begin{bmatrix} \dot{y} \\ \dot{\theta} l \end{bmatrix} + 2\omega_y\xi_y\begin{bmatrix} 1 & \varepsilon_{Cx} \\ \varepsilon_{Cx} & \varepsilon_{Cx}^2 + \lambda_C^2 \end{bmatrix}\begin{bmatrix} \dot{y} \\ \dot{\theta} l \end{bmatrix}$$
$$+ \omega_y^2\begin{bmatrix} 1 & \varepsilon_{kx} \\ \varepsilon_{kx} & \varepsilon_{kx}^2 + \lambda_k^2 \end{bmatrix}\begin{bmatrix} y \\ \theta l \end{bmatrix} + \omega_y^2 r_K\begin{bmatrix} 1 & \varepsilon_{Kx} \\ \varepsilon_{Kx} & \varepsilon_{Kx}^2 + \lambda_K^2 \end{bmatrix}\begin{bmatrix} y \\ \theta l \end{bmatrix} = -\begin{bmatrix} 1 & 0 \\ 0 & \lambda_M^2 \end{bmatrix}\begin{bmatrix} 1 \\ 0 \end{bmatrix}\ddot{u}_g, \tag{7}$$

where

- $\mathbf{U} = \begin{bmatrix} y \\ \theta l \end{bmatrix}$ relative displacement vector;
- $\mathbf{M} = \begin{bmatrix} 1 & 0 \\ 0 & \lambda_M^2 \end{bmatrix}$ mass matrix;
- $\mathbf{K} = \omega_y^2\begin{bmatrix} 1 & \varepsilon_{kx} \\ \varepsilon_{kx} & \varepsilon_{kx}^2 + \lambda_k^2 \end{bmatrix}$ structural stiffness matrix;
- $\mathbf{K_d} = \omega_y^2 r_K\begin{bmatrix} 1 & \varepsilon_{Kx} \\ \varepsilon_{Kx} & \varepsilon_{Kx}^2 + \lambda_K^2 \end{bmatrix}$ extra-structural stiffness matrix;
- $\mathbf{C_d} = 2\omega_y\xi_y\begin{bmatrix} 1 & \varepsilon_{Cx} \\ \varepsilon_{Cx} & \varepsilon_{Cx}^2 + \lambda_C^2 \end{bmatrix}$ extra-structural damping matrix;
- $\mathbf{I_g} = \begin{bmatrix} 1 \\ 0 \end{bmatrix}$ influence vector.

And can be compactly written as follows:

$$\mathbf{M}\ddot{\mathbf{U}} + (\alpha\mathbf{M} + \beta\mathbf{K})\dot{\mathbf{U}} + \mathbf{C_d}\dot{\mathbf{U}} + \mathbf{K}\mathbf{U} + \mathbf{K_d}\mathbf{U} = -\mathbf{M}\mathbf{I_g}\ddot{u}_g, \tag{8}$$

in which the controllable parameters are present in the matrices $\mathbf{C_d}$ and $\mathbf{K_d}$: ξ_y, r_K, denote the amount of available extra-structural damping and stiffness resources; ε_{Kx}, λ_K define the distribution of the extra-structural stiffness resources in plan; and ε_{Cx}, λ_C refer to the same properties for the extra-structural damping.

Premultiplying the terms of Equation (7) by the row vector $\dot{\mathbf{U}}^t = \begin{bmatrix} \dot{y} & \dot{\theta} l \end{bmatrix}$ and introducing the absolute displacement $Y = y + u_g$, Equation (9) applies:

$$\dot{Y}\ddot{Y} + \lambda_M^2 l^2\dot{\theta}\ddot{\theta} + \left(\alpha + \beta\omega_y^2 + 2\omega_y\xi_y\right)\dot{y}^2 + 2\omega_y l\left(\beta\omega_y\varepsilon_{kx} + 2\xi_y\varepsilon_{Cx}\right)\dot{y}\dot{\theta}$$
$$+ l^2\left(\alpha\lambda_M^2 + \beta\omega_y^2\left(\varepsilon_{kx}^2 + \lambda_k^2\right) + 2\omega_y\xi_y\left(\varepsilon_{Cx}^2 + \lambda_C^2\right)\right)\dot{\theta}^2 + \omega_y^2(1 + r_K)\dot{y}y + \omega_y^2 l(\varepsilon_{kx} + r_K\varepsilon_{Kx})(y\dot{\theta} + \dot{y}\theta) \tag{9}$$
$$+ \omega_y^2 l^2\left(\varepsilon_{kx}^2 + \lambda_k^2 + r_K\left(\varepsilon_{Kx}^2 + \lambda_K^2\right)\right)\theta\dot{\theta} = \dot{u}_g\ddot{Y}.$$

Integrating Equation (8) with respect to time between the beginning, t_{in}, and the end, t_{fin}, of the incoming seismic excitation, the energy balance can be expressed as Equation (10):

$$E_K + E_{\xi,y} + E_{\xi,y\theta} + E_{\xi,\theta} + E_{el} = E_{\text{in}}, \tag{10}$$

where

- $E_K = (1/2)\dot{Y}^2 + \lambda_M^2 l^2 \dot{\theta}^2$ kinetic energy;
- $E_{\xi,y} = (\alpha + \beta\omega_y^2 + 2\omega_y\xi_y)\int_{t_{in}}^{t_{fin}} \dot{y}^2 dt$ translational component of the dissipated energy;
- $E_{\xi,y\theta} = 2\omega_y l(\beta\omega_y\varepsilon_{kx} + 2\xi_y\varepsilon_{Cx})\int_{t_{in}}^{t_{fin}} \dot{y}\dot{\theta} dt$ torsional component of the dissipated energy;
- $E_{\xi,\theta} = l^2(\alpha\lambda_M^2 + \beta\omega_y^2(\varepsilon_{kx}^2 + \lambda_k^2) + 2\omega_y\xi_y(\varepsilon_{Cx}^2 + \lambda_C^2))\int_{t_{in}}^{t_{fin}} \dot{\theta}^2 dt$ rotational component of the dissipated energy;
- $E_{el} = (1/2)\omega_y^2(1 + r_K)y^2 + \omega_y^2 l(\varepsilon_{kx} + r_K\varepsilon_{Kx})y\theta + (1/2)\omega_y^2 l^2(\varepsilon_{kx}^2 + \lambda_k^2 + r_K(\varepsilon_{Kx}^2 + \lambda_K^2))\theta^2$ elastic energy;
- $E_{\text{in}} = \int_{t_{\text{in}}}^{t_{\text{fin}}} \dot{u}_g \dot{Y} dt$ input energy.

An expression in terms of the instantaneous powers (Equation (11)), where the meaning of the individual terms can be easily derived from the corresponding ones of Equation (10), can be written as follows:

$$P_K(t) + P_{\xi,y}(t) + P_{\xi,y\theta}(t) + P_{\xi,\theta}(t) + P_{el}(t) = P_{in}(t), \quad t \in [t_{in}, t_{fin}]. \tag{11}$$

Finally, note that the total dissipated energy can be expressed as

$$\begin{aligned} E_\xi &= \alpha\int_{t_{in}}^{t_{fin}} \dot{y}^2 dt + l^2\left(\alpha\lambda_M^2 + \beta\omega_y^2\lambda_k^2 + 2\omega_y\xi_y\lambda_C^2\right)\int_{t_{in}}^{t_{fin}} \dot{\theta}^2 dt + \left(\beta\omega_y^2\left(\int_{t_{in}}^{t_{fin}} \dot{y}^2 dt + \int_{t_{in}}^{t_{fin}} 2l\varepsilon_{kx}\dot{y}\dot{\theta} dt + \int_{t_{in}}^{t_{fin}} l^2\varepsilon_{kx}^2\dot{\theta}^2 dt\right)\right) \\ &\quad + \left(2\omega_y\xi_y\left(\int_{t_{in}}^{t_{fin}} \dot{y}^2 dt + \int_{t_{in}}^{t_{fin}} 2l\varepsilon_{Cx}\dot{y}\dot{\theta} dt + \int_{t_{in}}^{t_{fin}} l^2\varepsilon_{Cx}^2\dot{\theta}^2 dt\right)\right) \\ &= \alpha\int_{t_{in}}^{t_{fin}} \dot{y}^2 dt + l^2\left(\alpha\lambda_M^2 + \beta\omega_y^2\lambda_k^2 + 2\omega_y\xi_y\lambda_C^2\right)\int_{t_{in}}^{t_{fin}} \dot{\theta}^2 dt + \beta\omega_y^2\int_{t_{in}}^{t_{fin}} \left(\dot{y} + l\varepsilon_{kx}\dot{\theta}\right)^2 dt + 2\omega_y\xi_y\int_{t_{in}}^{t_{fin}} \left(\dot{y} + l\varepsilon_{Cx}\dot{\theta}\right)^2 dt, \end{aligned} \tag{12}$$

which shows how the instantaneous dissipated power is positive definite, and thus the dissipated energy is an increasing function of time.

3. Semi-Active Control Algorithms

In this study, the possibility to modify in real time the characteristics of extra-structural viscoelastic semi-active devices with respect to their nominal damping and stiffness values is considered. The idea is to develop algorithms based on the optimization of the energy balance components related to instantaneous powers, which indicate, at each instant, whether it is advantageous to increase or decrease the stiffness and damping values of the devices, depending on the dynamic state of the system together with the devices. This is possible both continuously adjusting the properties of devices, within values of interest, and selecting discrete properties (i.e., on and off states).

Variable stiffness and damping (VSD) devices [58, 59], hybrid semi-active actuators, and MR elastomers [60, 61] are examples of semi-active devices capable of altering both stiffness and damping properties. By incorporating magnetically sensitive particles into a polymer matrix, MR elastomers enable the simultaneous application of a magnetic field to control both properties. VSD devices can adjust damping and stiffness characteristics either independently or in tandem by using mechanisms such as variable fluid chambers or adaptive material effects. The degree of independent control over these variations depends on the device design. For example, MR elastomers typically exhibit coupled variations, whereas some hybrid actuators that combine MR and piezoelectric technology can achieve more independent tuning of stiffness and damping properties.

In the following, the stiffness and damping properties of a single semi-active device will be considered independent and operating in parallel. If they are connected in series, a Maxwell model should be used to describe the system's behavior [20]. However, this consideration does not compromise the proposed approach, as it is always possible to define equivalent (apparent) stiffness k_{eq} and damping c_{eq} values for the Maxwell model [20]. These values generally depend on the circular frequency that characterizes the system's motion, having stiffness k and damping factor c, and can be estimated using the fundamental frequency associated with the first mode of the asymmetric structural system (ω_1), through Equation (13) [20]:

$$k_{\text{eq}} = \frac{k}{\left(1 + \left((k/c)\omega_1\right)^2\right)}, \qquad c_{\text{eq}} = \frac{(k/c)\omega_1}{\left(1 + \left((k/c)\omega_1\right)^2\right)}. \tag{13}$$

As already stated, modifying the stiffness and damping parameters of the considered devices, K_{yi} and C_{yi}, in any number and plan-wise arrangement, allows for the variation of the six dynamic parameters of the problem: ξ_y, r_K, ε_K, λ_K, ε_C, λ_C, which are formally part of the two matrices $\mathbf{C_d}$ and $\mathbf{K_d}$. The first step is, therefore, to determine how the variation of these parameters affects the two matrices. In detail, limiting to the first-order terms, it is straightforward to define the variation of the considered matrices as follows:

$$\mathrm{d}\mathbf{C_d}\left(d\xi_y, d\varepsilon_{Cx}, d\lambda_C\right) = 2\omega_y\xi_y\begin{bmatrix} 0 & d\varepsilon_{Cx} \\ d\varepsilon_{Cx} & 2\varepsilon_{Cx}d\varepsilon_{Cx} + 2\lambda_C d\lambda_C \end{bmatrix} + 2\omega_y d\xi_y\begin{bmatrix} 1 & \varepsilon_{Cx} \\ \varepsilon_{Cx} & \varepsilon_{Cx}^2 + \lambda_C^2 \end{bmatrix}, \tag{14}$$

$$\mathrm{d}\mathbf{K_d}\left(dr_K, d\varepsilon_{Kx}, d\lambda_K\right) = \omega_y^2 r_K\begin{bmatrix} 0 & d\varepsilon_{Kx} \\ d\varepsilon_{Kx} & 2\varepsilon_{Kx}d\varepsilon_{Kx} + 2\lambda_K d\lambda_K \end{bmatrix} + \omega_y^2 dr_K\begin{bmatrix} 1 & \varepsilon_{Kx} \\ \varepsilon_{Kx} & \varepsilon_{Kx}^2 + \lambda_K^2 \end{bmatrix}. \tag{15}$$

In the following subsections, the expressions, related to the different energies and power components depending on the control parameters, will be described.

3.1. Maximization of Dissipated Energy. Equation (16) represents the variation in instantaneous power dissipated by the extra-structural devices. By expanding the terms of Equation (16), then, Equation (17) is defined

$$dP_\xi = \begin{Bmatrix} \dot{y} & \dot{\theta}l \end{Bmatrix} \cdot \mathrm{d}\mathbf{C_d} \cdot \begin{Bmatrix} \dot{y} \\ \dot{\theta}l \end{Bmatrix}, \tag{16}$$

$$\begin{aligned} dP_\xi &= 2\omega_y\begin{Bmatrix} \dot{y} & \dot{\theta}l \end{Bmatrix}\begin{bmatrix} d\xi_y & \xi_y d\varepsilon_{Cx} + \varepsilon_{Cx}d\xi_y \\ \xi_y d\varepsilon_{Cx} + \varepsilon_{Cx}d\xi_y & \xi_y\left(2\varepsilon_{Cx}d\varepsilon_{Cx} + 2\lambda_C d\lambda_C\right) + d\xi_y\left(\varepsilon_{Cx}^2 + \lambda_C^2\right) \end{bmatrix}\begin{Bmatrix} \dot{y} \\ \dot{\theta}l \end{Bmatrix} \\ &= 2\omega_y\begin{Bmatrix} \dot{y} & \dot{\theta}l \end{Bmatrix}\begin{bmatrix} d\xi_y & d\left(\xi_y\varepsilon_{Cx}\right) \\ d\left(\xi_y\varepsilon_{Cx}\right) & d\left[\xi_y\left(\varepsilon_{Cx}^2 + \lambda_C^2\right)\right] \end{bmatrix}\begin{Bmatrix} \dot{y} \\ \dot{\theta}l \end{Bmatrix} \\ &= 2\omega_y\begin{Bmatrix} \dot{y}d\xi_y + \dot{\theta}ld\left(\xi_y\varepsilon_{Cx}\right) & \dot{y}d\left(\xi_y\varepsilon_{Cx}\right) + \dot{\theta}ld\left[\xi_y\left(\varepsilon_{Cx}^2 + \lambda_C^2\right)\right] \end{Bmatrix}\begin{Bmatrix} \dot{y} \\ \dot{\theta}l \end{Bmatrix} \\ &= 2\omega_y\left(\dot{y}^2 d\xi_y + 2\dot{y}\dot{\theta}ld\left(\xi_y\varepsilon_{Cx}\right) + \dot{\theta}^2 l^2 d\left[\xi_y\left(\varepsilon_{Cx}^2 + \lambda_C^2\right)\right]\right). \end{aligned} \tag{17}$$

Using Equation (1a)–(1o) and the parameters defined in Section 2, the terms of Equation (17) can be expressed as a function of the damping coefficients of the extra-structural devices, as follows:

$$\xi_y = \frac{C_y}{2M\omega_y} = \frac{\sum_{i=1}^{N'} C_{yi}}{2M\omega_y} \longrightarrow d\xi_y = \frac{\sum_{i=1}^{N'} dC_{yi}}{2M\omega_y}, \tag{18a}$$

$$\xi_y\varepsilon_{Cx} = \frac{C_y}{2M\omega_y}\cdot\frac{\varepsilon_{Cx}}{l} = \frac{\sum_{i=1}^{N'} C_{yi}}{2M\omega_y}\cdot\frac{1}{l}\cdot\frac{\sum_{i=1}^{N'} C_{yi}\cdot x_{Ci}}{\sum_{i=1}^{N'} C_{yi}} = \frac{1}{2M\omega_y l}\sum_{i=1}^{N'} C_{yi}\cdot x_{Ci} \longrightarrow d\left(\xi_y\varepsilon_{Cx}\right) = \frac{\sum_{i=1}^{N'} dC_{yi}\cdot x_{Ci}}{2M\omega_y l}, \tag{18b}$$

$$\begin{aligned} \xi_y\left(\varepsilon_{Cx}^2 + \lambda_C^2\right) &= \frac{\sum_{i=1}^{N'} C_{yi}}{2M\omega_y}\cdot\left(\left(\frac{e_{Cx}}{l}\right)^2 + \left(\frac{\rho_{CD}}{l}\right)^2\right) = \frac{\sum_{i=1}^{N'} C_{yi}}{2M\omega_y}\cdot\frac{1}{l^2}\cdot\left(\left(\frac{\sum_{i=1}^{N'} C_{yi}\cdot x_{Ci}}{\sum_{i=1}^{N'} C_{yi}}\right)^2 + \frac{\sum_{i=1}^{N'} C_{yi}\cdot x_{Ci}^2 - C_y\cdot e_{Cx}^2}{\sum_{i=1}^{N'} C_{yi}}\right) \\ &= \frac{1}{2M\omega_y l^2}\cdot\left(\frac{\left(\sum_{i=1}^{N'} C_{yi}\cdot x_{Ci}\right)^2}{\sum_{i=1}^{N'} C_{yi}} + \sum_{i=1}^{N'} C_{yi}\cdot x_{Ci}^2 - \frac{\left(\sum_{i=1}^{N'} C_{yi}\cdot x_{Ci}\right)^2}{\sum_{i=1}^{N'} C_{yi}}\right) \\ &= \frac{\sum_{i=1}^{N'} C_{yi}\cdot x_{Ci}^2}{2M\omega_y l^2} \longrightarrow d\left[\xi_y\left(\varepsilon_{Cx}^2 + \lambda_C^2\right)\right] = \frac{\sum_{i=1}^{N'} dC_{yi}\cdot x_{Ci}^2}{2M\omega_y l^2}. \end{aligned} \tag{18c}$$

By substituting Equations (18a)–(18c) into (17), Equation (19) applies:

$$\begin{aligned} dP_{\xi} &= 2\omega_y \left(\dot{y}^2 \frac{\sum_{i=1}^{N'} dC_{yi}}{2M\omega_y} + 2\dot{y}\dot{\theta}l \frac{\sum_{i=1}^{N'} dC_{yi} \cdot x_{Ci}}{2M\omega_y l} + \dot{\theta}^2 l^2 \frac{\sum_{i=1}^{N'} dC_{yi} \cdot x_{Ci}^2}{2M\omega_y l^2} \right) \\ &= \frac{1}{M} \left(\dot{y}^2 \sum_{i=1}^{N'} dC_{yi} + 2\dot{y}\dot{\theta} \sum_{i=1}^{N'} dC_{yi} \cdot x_{Ci} + \dot{\theta}^2 \sum_{i=1}^{N'} dC_{yi} \cdot x_{Ci}^2 \right) \\ &= \frac{1}{M} \sum_{i=1}^{N'} dC_{yi} \cdot \left(\dot{y} + \dot{\theta} x_{Ci} \right)^2 = \frac{1}{M} \sum_{i=1}^{N'} dC_{yi} \cdot \left(\dot{y}_i \right)^2. \end{aligned} \tag{19}$$

Note that the term $\dot{y} + \dot{\theta} x_{Ci}$ corresponds to the relative velocity of the point where the i-th device is located, denoted as $\dot{y}_i$ in Equation (19).

To maximize the dissipated energy, it is necessary that dissipated power varies instantaneously so as to achieve the maximum positive value. Equation (19) highlights that, regardless of the dynamic state of the system, as well as the position and state of the individual device, this condition is to impose the maximum possible positive variation, within technological constraints, for the damping coefficients of the devices: $\max(dC_{yi})$. From a practical perspective, this means a very simple control algorithm: to maximize the dissipated energy, the semi-active devices must be configured so that their damping coefficients always take the maximum possible value (Equation (20)):

$$C_{yi} = C_{yi}^{(\max)}, \quad i = 1, 2, \ldots, N'. \tag{20}$$

3.2. Minimization of Elastic Energy. Equation (21) represents the variation in the instantaneous elastic power of the asymmetric system:

$$dP_{el} = \left\{ \dot{y} \;\; \dot{\theta}l \right\} \cdot d\left(\mathbf{K_d} \cdot \left\{ \begin{matrix} y \\ \theta l \end{matrix} \right\} \right) = \left\{ \dot{y} \;\; \dot{\theta}l \right\} \cdot \left(\mathrm{d}\mathbf{K_d} \cdot \left\{ \begin{matrix} y \\ \theta l \end{matrix} \right\} + \mathbf{K_d} \cdot d\left\{ \begin{matrix} y \\ \theta l \end{matrix} \right\} \right). \tag{21}$$

This equation takes into account both the variation in the stiffness matrix and system state in terms of the relative displacement to the activation of semi-active devices. Considering Equation (8), it is possible to expand the stiffness term related to the semi-active devices, as follows:

$$\mathbf{K_d} \cdot \left\{ \begin{matrix} y \\ \theta l \end{matrix} \right\} = -(\alpha\mathbf{M} + \beta\mathbf{K})\dot{\mathbf{U}} - \mathbf{C_d}\dot{\mathbf{U}} - \mathbf{K}\mathbf{U} - \mathbf{M}\ddot{\mathbf{U}} - \mathbf{M}\mathbf{I_g}\ddot{u}_g. \tag{22}$$

From Equation (22), considering that the variability of $\mathbf{K_d}$ has already been made explicit in the first term of Equations (21) and (23) applies:

$$d\left\{ \begin{matrix} y \\ \theta l \end{matrix} \right\} = -d\left(\mathbf{K_d^{-1}} \mathbf{C_d} \dot{\mathbf{U}} \right) = -\mathbf{K_d^{-1}} d\left(\mathbf{C_d} \right) \dot{\mathbf{U}}. \tag{23}$$

This result, together with Equation (15), leads to Equation (24) for the variation in the instantaneous elastic power:

$$\begin{aligned} dP_{el} &= \omega_y^2 \left\{ \dot{y} \;\; \dot{\theta}l \right\} \cdot \begin{bmatrix} dr_K & r_K d\varepsilon_{Kx} + \varepsilon_{Kx} dr_K \\ r_K d\varepsilon_{Kx} + \varepsilon_{Kx} dr_K & r_K \left(2\varepsilon_{Kx} d\varepsilon_{Kx} + 2\lambda_K d\lambda_K \right) + dr_K \left(\varepsilon_{Kx}^2 + \lambda_K^2 \right) \end{bmatrix} \cdot \left\{ \begin{matrix} y \\ \theta l \end{matrix} \right\} \\ &- \left\{ \dot{y} \;\; \dot{\theta}l \right\} \cdot d\left(\mathbf{C_d} \right) \cdot \left\{ \begin{matrix} \dot{y} \\ \dot{\theta}l \end{matrix} \right\} = dP_{el,K} + dP_{el,C}. \end{aligned} \tag{24}$$

The second term of Equation (24) has been developed in the case of the energy dissipation maximization algorithm (Subsection 3.1). Therefore, the focus will now be on developing the first term (Equation (25)):

$$dP_{el,K} = \omega_y^2 \left\{ \dot{y} \;\; \dot{\theta} l \right\} \cdot \begin{bmatrix} dr_K & d\left(r_K \varepsilon_{Kx}\right) \\ d\left(r_K \varepsilon_{Kx}\right) & d\left[r_K\left(\varepsilon_{Kx}^2 + \lambda_K^2\right)\right] \end{bmatrix} \cdot \begin{Bmatrix} y \\ \theta l \end{Bmatrix} = \omega_y^2 \left\{ \dot{y} dr_K + \dot{\theta} l d\left(r_K \varepsilon_{Kx}\right) \;\; \dot{y} d\left(r_K \varepsilon_{Kx}\right) + \dot{\theta} l \, d\left[r_K\left(\varepsilon_{Kx}^2 + \lambda_K^2\right)\right] \right\} \cdot \begin{Bmatrix} y \\ \theta l \end{Bmatrix} = \omega_y^2 \left(\dot{y} y dr_K + \left(y\dot{\theta} + \dot{y}\theta\right) l d\left(r_K \varepsilon_{Kx}\right) + \dot{\theta}\theta l^2 d\left[r_K\left(\varepsilon_{Kx}^2 + \lambda_K^2\right)\right] \right). \tag{25}$$

In this case as well, the parameters of Equation (25) can be expressed as a function of the extra-structural stiffness characteristics, as reported in Equations (26a)–(26c):

$$r_K = \frac{\sum_{i=1}^{N} K_{yi}}{\sum_{i=1}^{n} k_{yi}} \longrightarrow dr_K = \frac{\sum_{i=1}^{N} dK_{yi}}{M\omega_y^2}, \tag{26a}$$

$$\begin{aligned} r_K \varepsilon_{Kx} &= \frac{\sum_{i=1}^{N} K_{yi}}{\sum_{i=1}^{n} k_{yi}} \cdot \frac{e_{Kx}}{l} = \frac{\sum_{i=1}^{N} K_{yi}}{\sum_{i=1}^{n} k_{yi}} \cdot \frac{1}{l} \cdot \frac{\sum_{i=1}^{N} K_{yi} \cdot x_{Ki}}{\sum_{i=1}^{n} K_{yi}} \\ &= \frac{1}{M\omega_y^2 l} \sum_{i=1}^{N} K_{yi} \cdot x_{Ki} \longrightarrow d\left(r_K \varepsilon_{Kx}\right) = \frac{\sum_{i=1}^{N} dK_{yi} \cdot x_{Ki}}{M\omega_y^2 l}, \end{aligned} \tag{26b}$$

$$\begin{aligned} r_K\left(\varepsilon_{Kx}^2 + \lambda_K^2\right) &= \frac{\sum_{i=1}^{N} K_{yi}}{\sum_{i=1}^{n} k_{yi}} \left(\left(\frac{e_{Kx}}{l}\right)^2 + \left(\frac{\rho_K}{l}\right)^2 \right) = \frac{\sum_{i=1}^{N} K_{yi}}{M\omega_y^2} \cdot \frac{1}{l^2} \cdot \left(\left(\frac{\sum_{i=1}^{N} K_{yi} \cdot x_{Ki}}{\sum_{i=1}^{N} K_{yi}} \right)^2 + \frac{\sum_{i=1}^{N} K_{yi} \cdot x_{Ki}^2 - K_y \cdot e_{Kx}^2}{\sum_{i=1}^{N'} K_{yi}} \right) \\ &= \frac{1}{M\omega_y^2 l^2} \cdot \left(\frac{\left(\sum_{i=1}^{N} K_{yi} \cdot x_{Ki}\right)^2}{\sum_{i=1}^{N} K_{yi}} + \sum_{i=1}^{N} K_{yi} \cdot x_{Ki}^2 - \frac{\left(\sum_{i=1}^{N} K_{yi} \cdot x_{Ki}\right)^2}{\sum_{i=1}^{N} K_{yi}} \right) = \frac{\sum_{i=1}^{N} K_{yi} \cdot x_{Ki}^2}{M\omega_y^2 l^2} \longrightarrow d\left(r_K\left(\varepsilon_{Kx}^2 + \lambda_K^2\right) \right) \\ &= \frac{\sum_{i=1}^{N} dK_{yi} \cdot x_{Ki}^2}{M\omega_y^2 l^2}. \end{aligned} \tag{26c}$$

By substituting Equations (26a)–(26c) into (25), Equation (27) applies:

$$\begin{aligned} dP_{el,K} &= \omega_y^2 \left(\dot{y} y \frac{\sum_{i=1}^{N} dK_{yi}}{M\omega_y^2} + \left(y\dot{\theta} + \dot{y}\theta\right) l \frac{\sum_{i=1}^{N} dK_{yi} \cdot x_{Ki}}{M\omega_y^2 l} + \dot{\theta}\theta l^2 \frac{\sum_{i=1}^{N} dK_{yi} \cdot x_{Ki}^2}{M\omega_y^2 l^2} \right) \\ &= \frac{1}{M} \left(\dot{y} y \sum_{i=1}^{N} dK_{yi} + \left(y\dot{\theta} + \dot{y}\theta\right) \sum_{i=1}^{N} dK_{yi} \cdot x_{Ki} + \dot{\theta}\theta \sum_{i=1}^{N} dK_{yi} \cdot x_{Ki}^2 \right). \end{aligned} \tag{27}$$

By adding the second term of equation (24) and using equation (19), it follows that the following equation applies:

$$dP_{el} = \frac{1}{M}\left(\dot{y}y\sum_{i=1}^{N} dK_{yi} + (y\dot{\theta} + \dot{y}\theta)\sum_{i=1}^{N} dK_{yi}\cdot x_{Ki} + \dot{\theta}\theta\sum_{i=1}^{N} dK_{yi}\cdot x_{Ki}^2\right) - \frac{1}{M}\sum_{i=1}^{N'} dC_{yi}\cdot\left(\dot{y}_i\right)^2. \tag{28}$$

Compared to the previous case, the situation is more complex. In general, the contribution of the i-th device to the overall elastic power is

$$dP_{el,i} = \frac{1}{M}\left(\dot{y}y dK_{yi} + (y\dot{\theta} + \dot{y}\theta)\left(dK_{yi}\cdot x_{Ki}\right) + \dot{\theta}\theta\left(dK_{yi}\cdot x_{Ki}^2\right)\right) - \frac{1}{M}\, dC_{yi}\cdot\left(\dot{y}_i\right)^2. \tag{29}$$

It follows that the partial derivatives of the total instantaneous elastic power with respect, respectively, to the stiffness and damping value of the i-th generic device are

$$\frac{\delta P_{el,i}}{\delta C_{yi}} = \frac{dP_{el,i}}{dC_{yi}} = -\frac{1}{M}\left(\dot{y}_i\right)^2, \tag{30}$$

$$\begin{aligned}\frac{\delta P_{el,i}}{\delta K_{yi}} &= \frac{dP_{el,i}}{dK_{yi}} = \frac{1}{M}\left(\dot{y}y + (y\dot{\theta} + \dot{y}\theta)x_{Ki} + \dot{\theta}\theta x_{Ki}^2\right)\\ &= \frac{\dot{y}y}{M}\left(1 + \left(\frac{\dot{\theta}}{\dot{y}}\right)x_{Ki} + \left(\frac{\theta}{y}\right)x_{Ki} + \left(\frac{\dot{\theta}}{\dot{y}}\right)\left(\frac{\theta}{y}\right)x_{Ki}^2\right).\end{aligned} \tag{31}$$

Instantaneous power is the derivative of energy with respect to time: a negative value corresponds to a decrease in the amount of energy over time, as expressed in Equations (32) and (33):

$$-\frac{1}{M}\left(\dot{y}_i\right)^2 < 0, \tag{32}$$

$$\begin{aligned}&\frac{\dot{y}y}{M}\left(1 + \left(\frac{\dot{\theta}}{\dot{y}}\right)x_{Ki} + \left(\frac{\theta}{y}\right)x_{Ki} + \left(\frac{\dot{\theta}}{\dot{y}}\right)\left(\frac{\theta}{y}\right)x_{Ki}^2\right)\\ &= \frac{\dot{y}y}{M}\cdot\left(1 + \left(\frac{\theta x_{Ki}}{y}\right)\right)\cdot\left(1 + \left(\frac{\dot{\theta}x_{Ki}}{\dot{y}}\right)\right) < 0.\end{aligned} \tag{33}$$

Once these conditions are met, it will be advantageous to activate the maximum possible stiffness and damping value of the i-th device; otherwise, the minimum possible values should be used.

In the case of Equation (32), this condition is always satisfied, leading to the conclusion that, in order to reduce elastic energy, the available damping should be activated in every instance. This leads to the following rule for a control algorithm aimed at minimizing the elastic energy:

$$\begin{cases} K_{yi} = K_{yi}^{(\max)} \text{ if } \dot{y}y\cdot\left(1 + \left(\dfrac{\theta x_{Ki}}{y}\right)\right)\cdot\left(1 + \left(\dfrac{\dot{\theta}x_{Ki}}{\dot{y}}\right)\right) \le 0, \\ K_{yi} = K_{yi}^{(\min)} \text{ if } \dot{y}y\cdot\left(1 + \left(\dfrac{\theta x_{Ki}}{y}\right)\right)\cdot\left(1 + \left(\dfrac{\dot{\theta}x_{Ki}}{\dot{y}}\right)\right) > 0, \end{cases} \quad i = 1, 2, \ldots, N, \tag{34}$$

$$C_{yi} = C_{yi}^{(\max)}, \quad i = 1, 2, \ldots, N'. \tag{35}$$

Figure 2 shows the activation domain of the min/max stiffness values as defined by Equation (34).

3.3. Minimization of Kinetic Energy. Equation (36) represents the variation in the instantaneous kinetic power of the asymmetric system:

$$dP_K = \left\{\dot{Y} \;\; \dot{\theta}l\right\}\cdot d\left(\mathbf{M}\cdot\left\{\begin{matrix}\ddot{Y}\\ \ddot{\theta}l\end{matrix}\right\}\right). \tag{36}$$

Within the mass matrix, the terms related to the control of the semi-active devices do not explicitly appear. However, it is possible to express the product between the mass matrix and the vector of absolute accelerations from Equation (8), as follows:

$$\mathbf{M}\cdot\left\{\begin{matrix}\ddot{Y}\\ \ddot{\theta}l\end{matrix}\right\} = -(\alpha\mathbf{M} + \beta\mathbf{K})\dot{\mathbf{U}} - \mathbf{C_d}\dot{\mathbf{U}} - \mathbf{K}\mathbf{U} - \mathbf{K_d}\mathbf{U}. \tag{37}$$

By differentiating Equation (37) with respect to the controllable parameters, Equation (38) can be obtained:

$$d\left(\mathbf{M}\cdot\left\{\begin{matrix}\ddot{Y}\\ \ddot{\theta}l\end{matrix}\right\}\right) = -d\mathbf{C_d}\left\{\begin{matrix}\dot{y}\\ \dot{\theta}l\end{matrix}\right\} - d\mathbf{K}\left\{\begin{matrix}y\\ \theta l\end{matrix}\right\}, \tag{38}$$

which, written out, applies:

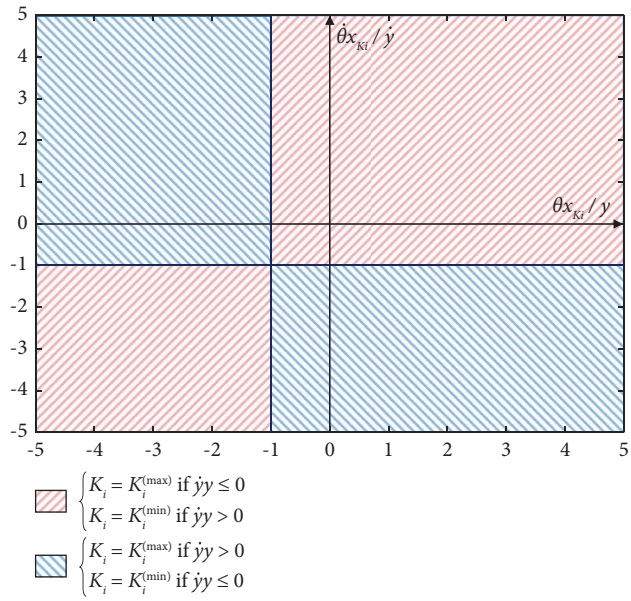

FIGURE 2: Elastic energy minimization activation domain for the stiffness value of the i-th device.

$$d\left(\mathbf{M}\cdot\begin{Bmatrix}\ddot{Y}\\ \ddot{\theta}l\end{Bmatrix}\right) = -2\omega_y\begin{bmatrix} d\xi_y & d\left(\xi_y\varepsilon_{Cx}\right) \\ d\left(\xi_y\varepsilon_{Cx}\right) & d\left(\xi_y\left(\varepsilon_{Cx}^2+\lambda_C^2\right)\right)\end{bmatrix}\begin{Bmatrix}\dot{y}\\ \dot{\theta}l\end{Bmatrix} - \omega_y^2\begin{bmatrix} dr_K & d\left(r_K\varepsilon_{Kx}\right) \\ d\left(r_K\varepsilon_{Kx}\right) & d\left(r_K\left(\varepsilon_{Kx}^2+\lambda_K^2\right)\right)\end{bmatrix}\begin{Bmatrix}y\\ \theta l\end{Bmatrix}. \tag{39}$$

Equation (39) allows us to write the variation in instantaneous kinetic power as a function of the six control parameters, as follows:

$$dP_K = \left\{\dot{Y}\ \ \dot{\theta}l\right\}\cdot\left(-2\omega_y\begin{bmatrix} d\xi_y & d\left(\xi_y\varepsilon_{Cx}\right) \\ d\left(\xi_y\varepsilon_{Cx}\right) & d\left(\xi_y\left(\varepsilon_{Cx}^2+\lambda_C^2\right)\right)\end{bmatrix}\begin{Bmatrix}\dot{y}\\ \dot{\theta}l\end{Bmatrix} - \omega_y^2\begin{bmatrix} dr_K & d\left(r_K\varepsilon_{Kx}\right) \\ d\left(r_K\varepsilon_{Kx}\right) & d\left(r_K\left(\varepsilon_{Kx}^2+\lambda_K^2\right)\right)\end{bmatrix}\begin{Bmatrix}y\\ \theta l\end{Bmatrix}\right), \tag{40}$$

which takes the following expanded form:

$$\begin{aligned} dP_K &= \left\{\dot{Y}\ \ \dot{\theta}l\right\}\cdot\left(-2\omega_y\begin{Bmatrix}\dot{y}d\xi_y + \dot{\theta}ld\left(\xi_y\varepsilon_{Cx}\right)\\ \dot{y}d\left(\xi_y\varepsilon_{Cx}\right) + \dot{\theta}ld\left(\xi_y\left(\varepsilon_{Cx}^2+\lambda_C^2\right)\right)\end{Bmatrix} - \omega_y^2\begin{Bmatrix} ydr_K + \theta ld\left(r_K\varepsilon_{Kx}\right)\\ yd\left(r_K\varepsilon_{Kx}\right) + \theta ld\left(r_K\left(\varepsilon_{Kx}^2+\lambda_K^2\right)\right)\end{Bmatrix}\right) \\ &= -\omega_y\cdot\left\{\dot{Y}\ \ \dot{\theta}l\right\}\begin{Bmatrix} 2\dot{y}d\xi_y + 2\dot{\theta}ld\left(\xi_y\varepsilon_{Cx}\right) + \omega_y ydr_K + \omega_y\theta ld\left(r_K\varepsilon_{Kx}\right)\\ 2\dot{y}d\left(\xi_y\varepsilon_{Cx}\right) + 2\dot{\theta}ld\left(\xi_y\left(\varepsilon_{Cx}^2+\lambda_C^2\right)\right) + \omega_y yd\left(r_K\varepsilon_{Kx}\right) + \omega_y\theta ld\left(r_K\left(\varepsilon_{Kx}^2+\lambda_K^2\right)\right)\end{Bmatrix} \\ &= -\omega_y\cdot\left(2\dot{y}\dot{Y}d\xi_y + 2\dot{\theta}\dot{Y}ld\left(\xi_y\varepsilon_{Cx}\right) + \omega_y y\dot{Y}dr_K + \omega_y\theta l\dot{Y}d\left(r_K\varepsilon_{Kx}\right) + 2\dot{y}\dot{\theta}ld\left(\xi_y\varepsilon_{Cx}\right) + 2\left(\dot{\theta}l\right)^2 d\left(\xi_y\left(\varepsilon_{Cx}^2+\lambda_C^2\right)\right)\right. \\ &\quad \left. + \omega_y y\dot{\theta}ld\left(r_K\varepsilon_{Kx}\right) + \omega_y\theta\dot{\theta}l^2 d\left(r_K\left(\varepsilon_{Kx}^2+\lambda_K^2\right)\right)\right). \end{aligned} \tag{41}$$

By substituting Equations (18a)–(18c) and (26a)–(26c) into Equations (41) and (42), we can obtain

$$dP_K = -\frac{\dot{y}\dot{Y}}{M}\sum_{i=1}^{N'} dC_{yi} - \frac{\dot{\theta}\dot{Y}}{M}\sum_{i=1}^{N'} dC_{yi}\cdot x_{Ci} - \frac{y\dot{Y}}{M}\sum_{i=1}^{N} dK_{yi} - \frac{\theta\dot{Y}}{M}\sum_{i=1}^{N} dK_{yi}\cdot x_{Ki} - \frac{\dot{y}\dot{\theta}}{M}\sum_{i=1}^{N'} dC_{yi}\cdot x_{Ci}$$
$$-\frac{\dot{\theta}^2}{M}\sum_{i=1}^{N'} dC_{yi}\cdot x_{Ci}^2 - \frac{y\dot{\theta}}{M}\sum_{i=1}^{N} dK_{yi}\cdot x_{Ki} - \frac{\theta\dot{\theta}}{M}\sum_{i=1}^{N} dK_{yi}\cdot x_{Ki}^2 \tag{42}$$
$$= -\frac{1}{M}\cdot\left(\sum_{i=1}^{N'}\left(\dot{y}\dot{Y} + \dot{\theta}\dot{Y}x_{Ci} + \dot{y}\dot{\theta}x_{Ci} + \dot{\theta}^2 x_{Ci}^2\right)dC_{yi} + \sum_{i=1}^{N}\left(y\dot{Y} + \theta\dot{Y}x_{Ki} + y\dot{\theta}x_{Ki} + \theta\dot{\theta}x_{Ki}^2\right)dK_{yi}\right).$$

Therefore, similarly to the previous criterion, by considering the contribution of the devices and calculating the partial derivatives of the instantaneous kinetic power with respect to the damping and stiffness values of the i-th device, Equations (43) and (44) can be derived:

$$\frac{\delta P_K}{\delta C_{yi}} = -\frac{1}{M}\left(\dot{y}\dot{Y} + (\dot{Y}+\dot{y})\dot{\theta}x_{Ci} + \dot{\theta}^2 x_{Ci}^2\right), \quad i = 1, 2, \ldots, N', \tag{43}$$

$$\frac{\delta P_K}{\delta K_{yi}} = -\frac{1}{M}\left(\dot{y}\dot{Y} + \dot{Y}\theta x_{Ki} + y\dot{\theta}x_{Ki} + \theta\dot{\theta}x_{Ki}^2\right), \quad i = 1, 2, \ldots, N. \tag{44}$$

Aiming to reduce the instantaneous kinetic power, both the derivatives must be negative:

$$\frac{\delta P_K}{\delta C_{yi}} < 0 \longrightarrow -\frac{\dot{y}\dot{Y}}{M}\left(1 + \left(1+\frac{\dot{y}}{\dot{Y}}\right)\frac{\dot{\theta}x_{Ci}}{\dot{y}} + \frac{\dot{y}}{\dot{Y}}\left(\frac{\dot{\theta}x_{Ci}}{\dot{y}}\right)^2\right) < 0, \quad i = 1, 2, \ldots, N', \tag{45}$$

$$\frac{\delta P_K}{\delta K_{yi}} = -\frac{y\dot{Y}}{M}\left(1 + \frac{\theta x_{Ki}}{y} + \frac{\dot{\theta}x_{Ki}}{\dot{Y}} + \frac{\theta x_{Ki}}{y}\frac{\dot{\theta}x_{Ki}}{\dot{Y}}\right) = -\frac{y\dot{Y}}{M}\left(1+\frac{\theta x_{Ki}}{y}\right)\left(1+\frac{\dot{\theta}x_{Ki}}{\dot{Y}}\right) < 0, \quad i = 1, 2, \ldots, N. \tag{46}$$

Thus, the control algorithm for minimizing kinetic energy applies:

$$\begin{cases} C_{yi} = C_{yi}^{(\max)} \text{ if } \dot{y}\dot{Y}\cdot\left(1 + \left(1+\frac{\dot{y}}{\dot{Y}}\right)\frac{\dot{\theta}x_{Ci}}{\dot{y}} + \frac{\dot{y}}{\dot{Y}}\left(\frac{\dot{\theta}x_{Ci}}{\dot{y}}\right)^2\right) \geq 0, \\ C_{yi} = C_{yi}^{(\min)} \text{ if } \dot{y}\dot{Y}\cdot\left(1 + \left(1+\frac{\dot{y}}{\dot{Y}}\right)\frac{\dot{\theta}x_{Ci}}{\dot{y}} + \frac{\dot{y}}{\dot{Y}}\left(\frac{\dot{\theta}x_{Ci}}{\dot{y}}\right)^2\right) < 0, \end{cases} \quad i = 1, 2, \ldots N', \tag{47}$$

$$\begin{cases} K_{yi} = K_{yi}^{(\max)} \text{ if } y\dot{Y}\left(1+\frac{\theta x_{Ki}}{y}\right)\left(1+\frac{\dot{\theta}x_{Ki}}{\dot{Y}}\right) \geq 0, \\ K_{yi} = K_{yi}^{(\min)} \text{ if } y\dot{Y}\left(1+\frac{\theta x_{Ki}}{y}\right)\left(1+\frac{\dot{\theta}x_{Ki}}{\dot{Y}}\right) < 0, \end{cases} \quad i = 1, 2, \ldots N. \tag{48}$$

Figures 3 and 4 show, respectively, the activation domains for the values of both damping and stiffness, related to Equations (47) and (48).

3.4. Minimization of Input Energy. Equation (42) expresses the instantaneous input power, which takes an even simpler form than in previous cases, as does not involve any matrix representing the system's dynamic properties:

$$dP_{in} = \left\{ \dot{u}_g \;\; 0 \right\} \cdot d \left\{ \begin{matrix} \ddot{Y} \\ \ddot{\theta} l \end{matrix} \right\} = \dot{u}_g d\ddot{Y}. \tag{49}$$

Using Equation (8), the differential term of Equation (49) can be written as follows:

$$d \left\{ \begin{matrix} \ddot{Y} \\ \ddot{\theta} l \end{matrix} \right\} = -\mathbf{M}^{-1} \left(d\mathbf{C_d} \left\{ \begin{matrix} \dot{y} \\ \dot{\theta} l \end{matrix} \right\} + d\mathbf{K_d} \left\{ \begin{matrix} y \\ \theta l \end{matrix} \right\} \right), \tag{50}$$

by performing the inversion of the mass matrix and using Equations (14) and (15), Equation (51) can be written:

$$d \left\{ \begin{matrix} \ddot{Y} \\ \ddot{\theta} l \end{matrix} \right\} = -2\omega_y \begin{bmatrix} d\xi_y & d\left(\xi_y \varepsilon_{Cx}\right) \\ \dfrac{d\left(\xi_y \varepsilon_{Cx}\right)}{\lambda_M^2} & \dfrac{d\left(\xi_y \left(\varepsilon_{Cx}^2 + \lambda_C^2\right)\right)}{\lambda_M^2} \end{bmatrix} \left\{ \begin{matrix} \dot{y} \\ \dot{\theta} l \end{matrix} \right\} - \omega_y^2 \begin{bmatrix} dr_K & d\left(r_K \varepsilon_{Kx}\right) \\ \dfrac{d\left(r_K \varepsilon_{Kx}\right)}{\lambda_M^2} & \dfrac{d\left(r_K \left(\varepsilon_{Kx}^2 + \lambda_K^2\right)\right)}{\lambda_M^2} \end{bmatrix} \left\{ \begin{matrix} y \\ \theta l \end{matrix} \right\}. \tag{51}$$

This relationship allows us to express the variation in instantaneous input power as a function of the six control parameters, as follows:

$$dP_{in} = \left\{ \dot{u}_g \;\; 0 \right\} \cdot \left(-2\omega_y \begin{bmatrix} d\xi_y & d\left(\xi_y \varepsilon_{Cx}\right) \\ \dfrac{d\left(\xi_y \varepsilon_{Cx}\right)}{\lambda_M^2} & \dfrac{d\left(\xi_y \left(\varepsilon_{Cx}^2 + \lambda_C^2\right)\right)}{\lambda_M^2} \end{bmatrix} \left\{ \begin{matrix} \dot{y} \\ \dot{\theta} l \end{matrix} \right\} - \omega_y^2 \begin{bmatrix} dr_K & d\left(r_K \varepsilon_{Kx}\right) \\ \dfrac{d\left(r_K \varepsilon_{Kx}\right)}{\lambda_M^2} & \dfrac{d\left(r_K \left(\varepsilon_{Kx}^2 + \lambda_K^2\right)\right)}{\lambda_M^2} \end{bmatrix} \left\{ \begin{matrix} y \\ \theta l \end{matrix} \right\} \right), \tag{52}$$

which takes the following expanded form:

$$\begin{aligned} dP_{in} &= \left\{ \dot{u}_g \;\; 0 \right\} \cdot \left(-2\omega_y \left\{ \begin{matrix} \dot{y} d\xi_y + \dot{\theta} l d\left(\xi_y \varepsilon_{Cx}\right) \\ \dfrac{1}{\lambda_M^2} \left(\dot{y} d\left(\xi_y \varepsilon_{Cx}\right) + \dot{\theta} l d\left(\xi_y \left(\varepsilon_{Cx}^2 + \lambda_C^2\right)\right)\right) \end{matrix} \right\} - \omega_y^2 \left\{ \begin{matrix} y dr_K + \theta l d\left(r_K \varepsilon_{Kx}\right) \\ \dfrac{1}{\lambda_M^2} \left(y d\left(r_K \varepsilon_{Kx}\right) + \theta l d\left(r_K \left(\varepsilon_{Kx}^2 + \lambda_K^2\right)\right)\right) \end{matrix} \right\} \right) \\ &= -\omega_y \cdot \left\{ \dot{u}_g \;\; 0 \right\} \cdot \left\{ \begin{matrix} 2\dot{y} d\xi_y + 2\dot{\theta} l d\left(\xi_y \varepsilon_{Cx}\right) + \omega_y y dr_K + \omega_y \theta l d\left(r_K \varepsilon_{Kx}\right) \\ \dfrac{1}{\lambda_M^2} \left(2\dot{y} d\left(\xi_y \varepsilon_{Cx}\right) + 2\dot{\theta} l d\left(\xi_y \left(\varepsilon_{Cx}^2 + \lambda_C^2\right)\right) + \omega_y y d\left(r_K \varepsilon_{Kx}\right) + \omega_y \theta l d\left(r_K \left(\varepsilon_{Kx}^2 + \lambda_K^2\right)\right)\right) \end{matrix} \right\} \\ &= -\omega_y \cdot \left(2\dot{y} \dot{u}_g d\xi_y + 2\dot{\theta} l \dot{u}_g d\left(\xi_y \varepsilon_{Cx}\right) + \omega_y y \dot{u}_g dr_K + \omega_y \theta l \dot{u}_g d\left(r_K \varepsilon_{Kx}\right)\right). \end{aligned} \tag{53}$$

By substituting equations (18a)–(18c) and (26a)–(26c) into equation (53), it follows that the following equation applies:

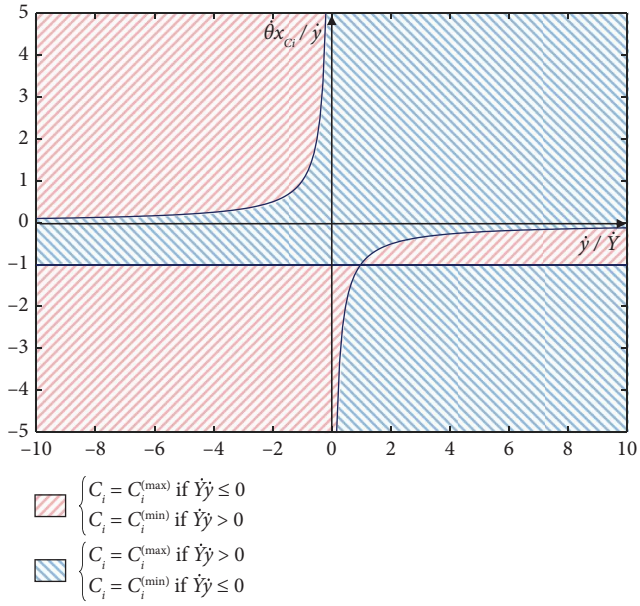

FIGURE 3: Kinetic energy minimization activation domain for the damping value of the i-th device.

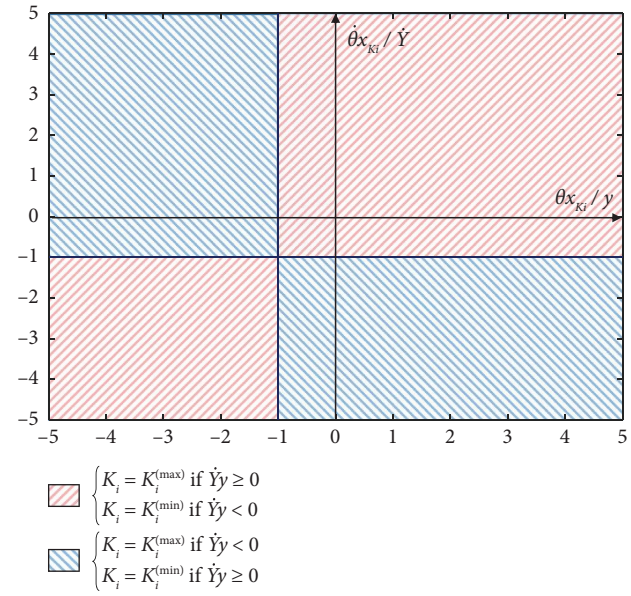

FIGURE 4: Kinetic energy minimization activation domain for the stiffness value of the i-th device.

$$dP_{in} = -\frac{\dot{y}\dot{u}_g}{M}\sum_{i=1}^{N'} dC_{yi} - \frac{\dot{\theta}\dot{u}_g}{M}\sum_{i=1}^{N'} dC_{yi}\cdot x_{Ci} - \frac{y\dot{u}_g}{M}\sum_{i=1}^{N} dK_{yi} - \frac{\theta\dot{u}_g}{M}\sum_{i=1}^{N} dK_{yi}\cdot x_{Ki} = -\frac{1}{M}\left(\sum_{i=1}^{N'} \dot{u}_g\left(\dot{y}+\dot{\theta}x_{Ci}\right)dC_{yi} + \sum_{i=1}^{N} \dot{u}_g\left(y+\theta x_{Ki}\right)dK_{yi}\right). \tag{54}$$

Similarly to the previous cases, the following partial derivatives are obtained:

$$\frac{\delta P_{in}}{\delta C_{yi}} = -\frac{1}{M}\dot{u}_g\left(\dot{y} + \dot{\theta}x_{Ci}\right), \quad i = 1, 2, \ldots, N', \tag{55}$$

$$\frac{\delta P_{in}}{\delta K_{yi}} = -\frac{1}{M}\dot{u}_g\left(y + \theta x_{Ki}\right), \quad i = 1, 2, \ldots, N. \tag{56}$$

To ensure that the device's contribution leads to a reduction of the input power, both these derivatives must be negative:

$$\frac{\delta P_{in}}{\delta C_{yi}} < 0 \longrightarrow -\frac{1}{M}\dot{u}_g^2\left(\frac{\dot{y}}{\dot{u}_g} + \frac{\dot{\theta}x_{Ci}}{\dot{u}_g}\right) < 0 \longrightarrow \frac{\dot{y}}{\dot{u}_g} + \frac{\dot{\theta}x_{Ci}}{\dot{u}_g} > 0, \quad i = 1, 2, \ldots, N', \tag{57}$$

$$\frac{\delta P_{in}}{\delta K_{yi}} < 0 \longrightarrow -\frac{1}{M}\dot{u}_g^2\left(\frac{y}{\dot{u}_g} + \frac{\theta x_{Ki}}{\dot{u}_g}\right) < 0 \longrightarrow \frac{y}{\dot{u}_g} + \frac{\theta x_{Ki}}{\dot{u}_g} > 0, \quad i = 1, 2, \ldots, N, \tag{58}$$

which lead to the following semi-active control algorithm aimed at reducing the input energy:

$$\begin{cases} C_{yi} = C_{yi}^{(\max)} \text{ if } \dfrac{\dot{y}}{\dot{u}_g} + \dfrac{\dot{\theta}x_{Ci}}{\dot{u}_g} \geq 0, \\ \\ C_{yi} = C_{yi}^{(\min)} \text{ if } \dfrac{\dot{y}}{\dot{u}_g} + \dfrac{\dot{\theta}x_{Ci}}{\dot{u}_g} < 0, \end{cases} \quad i = 1, 2, \ldots, N', \tag{59}$$

$$\begin{cases} K_{yi} = K_{yi}^{(\max)} \text{ if } \dfrac{y}{\dot{u}_g} + \dfrac{\theta x_{Ci}}{\dot{u}_g} \geq 0, \\ \\ K_{yi} = K_{yi}^{(\min)} \text{ if } \dfrac{y}{\dot{u}_g} + \dfrac{\theta x_{Ci}}{\dot{u}_g} < 0, \end{cases} \quad i = 1, 2, \ldots, N. \tag{60}$$

Figures 5 and 6 show, respectively, the domains related to the damping and stiffness control algorithms, as expressed by Equations (59) and (60).

3.5. Summary of the Proposed Semi-Active Control Algorithms. For the sake of clarity, the laws identified for the considered algorithms are summarized in Table 1, where the variations in both damping and stiffness properties of the viscoelastic semi-active devices are shown and the control laws are formulated by using non-dimensional parameters. These parameters describe the system's instantaneous dynamic behavior and along with the positions of the generic i-th extra-structural resources of stiffness and damping, expressed in a dimensionless form, respectively, as ε_{Ki} and ε_{Ci}, help to identify the devices for which it is appropriate, according to the algorithm's objective, to increase or reduce these properties. Apart from the extra-structural damping laws for algorithms that maximize dissipated energy and minimize elastic energy, the other relationships depend on a significant number of parameters. These include displacement and velocity components, both translational and rotational, absolute translational velocity, and ground velocity.

To provide a concise illustration of how each individual algorithm operates, Figures 7, 8, and 9 show the semi-active control actions, $(\Delta K_i, \Delta C_i)$, for elastic, kinetic, and input energy algorithms, respectively, since the dissipated energy algorithm corresponds to a passive control approach. For the sake of simplicity, these figures refer to the case of two viscoelastic devices placed at the edge of the structural system (i.e., $\varepsilon_{Ki} = \varepsilon_{Ci} = \pm 1/2$). Specifically, assuming the positive directions of translational motion components in terms of both displacement and velocity as reported in the plots, Figures 7, 8, and 9 show how the different values of the torsional component influence the control algorithm's behavior on each individual device: Figures 7(a) and 9(a) refer to a limited intensity of the torsional displacement component; Figures 7(b), 7(c), 9(b), and 9(c) refer to a significant value of the torsional displacement component, matching and opposing the sign of the translational component.

4. Effectiveness of the Proposed Semi-Active Control Algorithms

With the aim to verify the effectiveness of the proposed semi-active control algorithms, summarized in Table 1, the seismic responses of asymmetric systems with variable stiffness geometry were studied under a wide set of seismic excitations with very different dynamic characteristics. In detail, Tables 2 and 3 summarize the main properties of the 85 accelerograms [62, 63] considered in the numerical investigation, where the excitations labeled from 1 to 45 are far-field records with different values of the PGA to PGV ratios and those from 46 to 85 are near-fault records characterized by a significant impulsive component.

The considered structural systems will be characterized by the following independent and deterministic parameters: T_y, ε_{kx}, λ_k, λ_M, α, and β. Specifically, the value of the decoupled translational period will be varied within the range $T_y \in [0\,\text{s}, 2\,\text{sec}]$, while three values will be considered for the dimensionless structural eccentricity: $\varepsilon_{kx} \in \{0.02, 0.05, 0.10\}$. The dimensionless radius of gyration for stiffness is calculated as a function of the structural

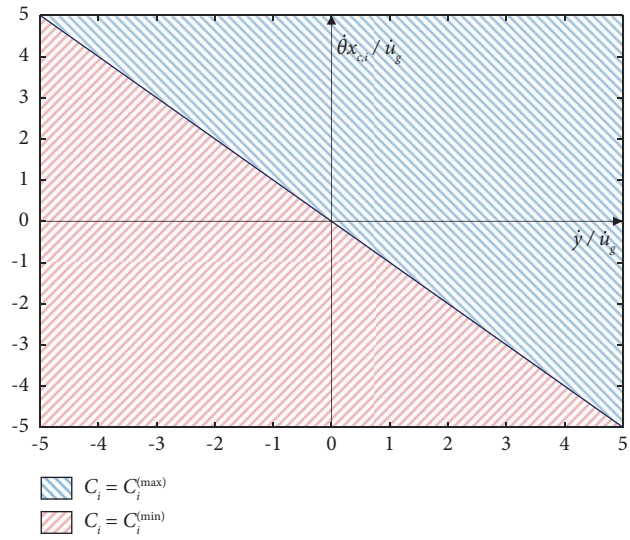

FIGURE 5: Input energy minimization control algorithm for the damping value of the i-th device.

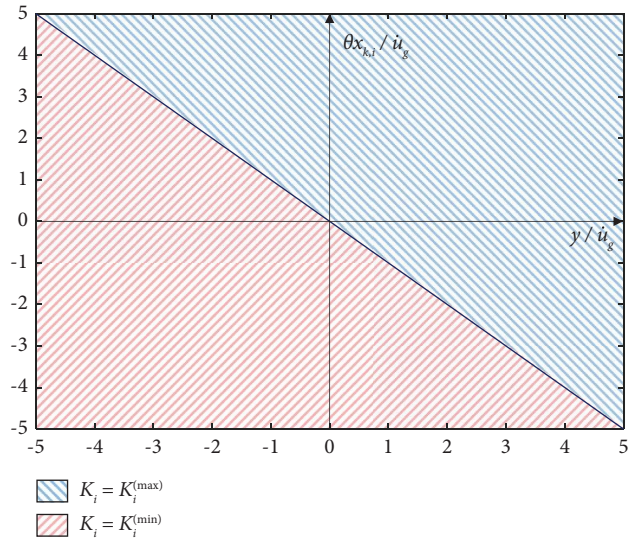

FIGURE 6: Input energy minimization control algorithm for the stiffness value of the i-th device.

eccentricity through the following relation: $\lambda_k = 1/2 - \varepsilon_{kx}$. This relationship is obtained by modeling the stiffness distribution through two equivalent elements positioned at the same distance, $l/2$, from the center of mass. With this schematic representation, the result derives directly from the application of the Parallel *Axis* Theorem. The corresponding parameter for the mass is set to $\lambda_M = \sqrt{1.25/12}$, corresponding to a rectangular system with an aspect ratio of 1/2 with a uniformly distributed mass. Finally, as already mentioned, the Rayleigh inherent damping parameters (α and β) are adjusted case by case to achieve a 2% damping coefficient on the system's two modes.

Table 4, for example, reports the mechanical characteristics of the investigated uncontrolled systems, including the periods and the components of the modes related only to the translational period $T_y = 1$ sec together with the three considered eccentricity values. In this way, the significance of the analyzed cases is clearly highlighted. In fact, under the condition $\varepsilon_{kx} = 0.02$, the system exhibits two well-separated modes: the first one is translational, while the second one is rotational. This separation decreases in the condition $\varepsilon_{kx} = 0.05$, while in the condition $\varepsilon_{kx} = 0.10$, the system is characterized by a strong coupling between the two motion components. The selection of these three eccentricity values thus allows for evaluating the control system's performance in three distinct and meaningful scenarios.

Regarding the semi-active devices, five elements were considered, arranged as shown in Figure 10, capable of adjusting both their damping and stiffness properties between zero and specific maximum values. The maximum

Table 1: Semi-active control laws for the different considered algorithms.

Objective of the algorithm	Extra-structural damping	Extra-structural stiffness
Maximization of dissipated energy	$\Delta C_i > 0$ in any condition	No control
Minimization of elastic energy	$\Delta C_i > 0$ in any condition	$\begin{cases} \Delta K_i \geq 0 \text{ if } \dot{y}y \cdot (1 + ((\theta x_{Ki})/y)) \cdot (1 + ((\dot{\theta} x_{Ki})/\dot{y})) \leq 0 \\ \Delta K_i < 0 \text{ if } \dot{y}y \cdot (1 + ((\theta x_{Ki})/y)) \cdot (1 + ((\dot{\theta} x_{Ki})/\dot{y})) > 0 \end{cases}$
Minimization of kinetic energy	$\begin{cases} \Delta C_i \geq 0 \text{ if } \dot{y}\dot{Y} \cdot (1 + (1 + \dot{y}/\dot{Y})((\dot{\theta} x_{Ci})/\dot{y}) + (\dot{y}/\dot{Y})((\dot{\theta} x_{Ci})/\dot{y})^2) \geq 0 \\ \Delta C_i < 0 \text{ if } \dot{y}\dot{Y} \cdot (1 + (1 + \dot{y}/\dot{Y})((\dot{\theta} x_{Ci})/\dot{y}) + (\dot{y}/\dot{Y})((\dot{\theta} x_{Ci})/\dot{y})^2) < 0 \end{cases}$	$\begin{cases} \Delta K_i \geq 0 \text{ if } y\dot{Y}(1 + (\theta x_{Ki})/y)(1 + (\dot{\theta} x_{Ki})/\dot{Y}) \geq 0 \\ \Delta K_i < 0 \text{ if } y\dot{Y}(1 + (\theta x_{Ki})/y)(1 + (\dot{\theta} x_{Ki})/\dot{Y}) < 0 \end{cases}$
Minimization of input energy	$\begin{cases} \Delta C_i \geq 0 \text{ if } (\dot{y}/\dot{u}_g) + ((\dot{\theta} x_{Ci})/\dot{u}_g) \geq 0 \\ \Delta C_i < 0 \text{ if } (\dot{y}/\dot{u}_g) + ((\dot{\theta} x_{Ci})/\dot{u}_g) < 0 \end{cases}$	$\begin{cases} \Delta K_i \geq 0 \text{ if } (y/\dot{u}_g) + ((\theta x_{Ci})/\dot{u}_g) \geq 0 \\ \Delta K_i < 0 \text{ if } (y/\dot{u}_g) + ((\theta x_{Ci})/\dot{u}_g) < 0 \end{cases}$

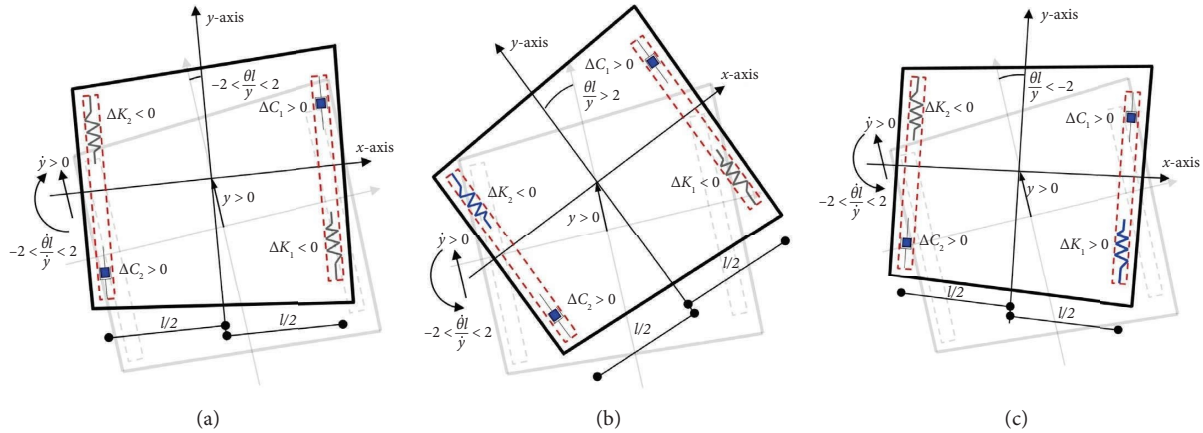

FIGURE 7: Semi-active control for the elastic energy minimization algorithm with varying parameters $\theta l/y$.

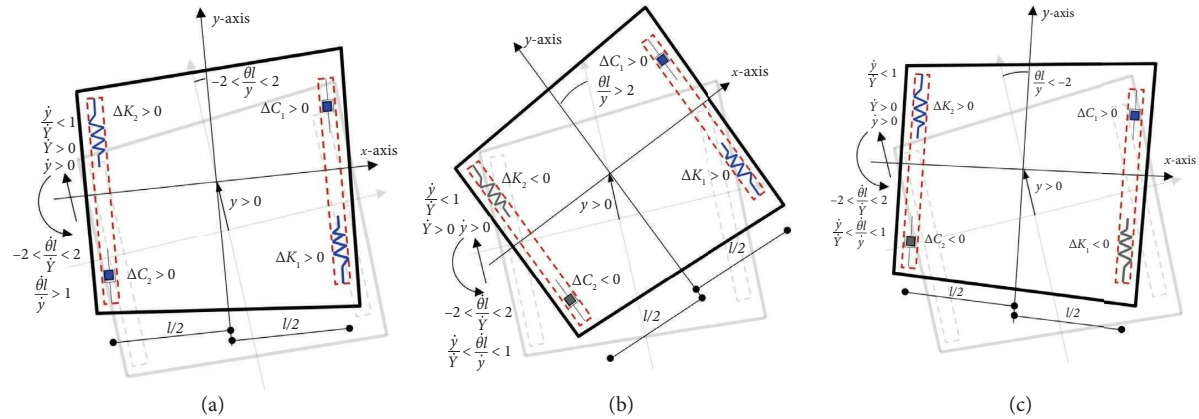

FIGURE 8: Semi-active control for the kinetic energy minimization algorithm with varying parameters $\theta l/y$, $\dot{\theta} l/\dot{y}$.

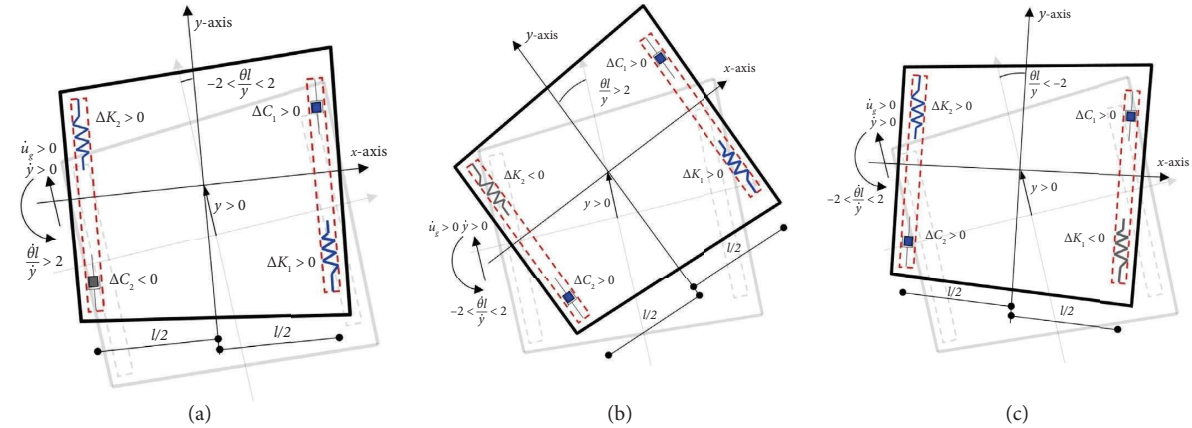

FIGURE 9: Semi-active control for the input energy minimization algorithm with varying parameters $\theta l/y$.

values for both damping and stiffness properties are set to be compatible with engineering applications. Specifically, the maximum damping value is designed to achieve an extra-structural equivalent damping coefficient equal to 10% of the critical damping factor in the translational mode, assuming no eccentricity and that all semi-active devices are activated. As for stiffness, five different levels were provided for the maximum value, with increments ranging between 10% and 50% of the original structural value: $r_K = K_y/k_y \in \{0.1, 0.2, 0.3, 0.4, 0.5\}$.

Table 2: Considered far-field seismic records.

#	Earthquake	Date	Mg	PGA (m/s^2)	Site	Epic. dist. (Km)	Comp.	PGA/PGV (s^{-1})	Specific energy density (m^2/s)	Soil (EC 8 class)
1	Parkfield California	June 27, 1966	5.6	2.594	Temblor no. 2	7	N65W	18.87	0.0172	A
2	Parkfield California	June 27, 1966	5.6	4.176	Cholame, Shandon no. 5	5	N85W	16.39	0.0622	A
3	San Francisco California	Mar. 22, 1957	5.2	1.009	Golden Gate Park	11	S80E	25.00	0.0012	A
4	San Francisco California	Mar. 22, 1957	5.2	0.823	State Bldg., S.F.	17	S09E	20.83	0.0022	B
5	Helena Montana	Oct. 31, 1935	6	1.410	Carroll College	8	N00E	19.61	0.0022	A
6	Lytle Creek	Sep. 12, 1970	5.4	1.910	Wrightwood, California	15	S25W	18.87	0.0032	A
7	Oroville California	Aug. 1, 1975	5.7	0.807	Seismogr. StationOroville	13	N53W	16.39	0.0012	A
8	San Fernando California	Feb. 9, 1971	6.4	10.350	Pacomia Dam	4	S74W	17.86	0.3092	A
9	San Fernando California	Feb. 9, 1971	6.4	1.407	Lake Hughes, Station 4	26	S21W	16.67	0.0062	A
10	NahanniN.W.T., Canada	Dec. 23, 1985	6.9	10.610	Site 1, Iverson	7.5	LONG	23.26	0.1342	A
11	Central Honshu Japan	Feb. 26, 1971	5.5	1.453	Yoneyama bridge	27	TRANS	25.00	0.0012	B
12	Near E. Coast of Honshu, Japan	May. 11, 1972	5.8	1.401	Kushiro CentralWharf	33	N00E	24.39	0.0032	B
13	Honshu Japan	Apr. 5, 1966	5.4	2.604	Hoshina–A	4	N00E	22.73	0.0032	B
14	Monte Negro Yugoslavia	Apr. 9, 1979	5.4	0.405	Albatros Hotel, Ulcinj	12.5	N00E	25.64	0.0002	A
15	Banja Luka Yugoslavia	Aug. 13, 1981	6.1	0.709	Seism. Station, Banja Luka	8.5	N90W	22.73	0.0012	A
16	Imperial Valley California	May 18, 1940	6.6	3.348	El Centro	8	S00E	9.26	0.2132	B
17	Kern County California	July 21, 1952	7.6	1.727	Taft Lincoln School Tunnel	56	S69E	10.42	0.0982	A
18	Kern County California	July 21, 1952	7.6	1.500	Taft Lincoln School Tunnel	56	N21E	9.01	0.0782	A
19	Borrego Mtn. California	April 8, 1968	6.5	0.446	San Onofre SCE power Plant	122	N57W	10.87	0.0082	B
20	Borrego Mtn. California	April 8, 1968	6.5	0.393	San Onofre SCE power Plant	122	N33E	10.99	0.0042	B
21	San Fernando California	Feb. 9, 1971	6.4	1.448	3838 Lankershim Blvd., L.A.	24	S90W	9.35	0.0272	A
22	San Fernando California	Feb. 9, 1971	6.4	2.031	Hollywood Storage P.E. Lot, L.A.	35	N90E	10.10	0.1322	B
23	San Fernando California	Feb. 9, 1971	6.4	1.590	3407 6th Street, L.A.	39	N90E	10.10	0.0772	B
24	San Fernando California	Feb. 9, 1971	6.4	1.735	Griffith Park Observatory, L.A.	31	S00W	8.47	0.0502	A
25	San Fernando California	Feb. 9, 1971	6.4	1.920	234 Figueroa st., L.A.	41	N37E	11.90	0.0662	B
26	Near E. Coast of Honshu, Japan	Nov. 16, 1974	6.1	0.677	Kashima Harbor works	38	N00E	9.43	0.0052	B
27	Near E. Coast of Honshu, Japan	Aug. 2, 1971	7	0.746	Kushiro Central Wharf	196	N90E	10.99	0.0092	B

Table 2: Continued.

#	Earthquake	Date	Mg	PGA (m/s^2)	Site	Epic. dist. (Km)	Comp.	PGA/PGV (s^{-1})	Specific energy density (m^2/s)	Soil (EC 8 class)
28	Monte Negro Yugoslavia	Apr. 15, 1979	7	1.650	Albatros Hotel, Ulcinj	17	N00E	8.40	0.0502	A
29	Mexico earthquake	Sept. 19 1985	8.1	1.012	El Suchil, Guerrero Array	230	S00E	8.85	0.0172	A
30	Mexico earthquake	Sept. 19 1985	8.1	1.185	La Villita, Guerrero Array	44	N90E	11.63	0.0272	A
31	Long Beach California	Mar. 10, 1933	6.3	0.938	Subway Terminal, L.A.	59	N51W	4.22	0.1752	A
32	Long Beach California	Mar. 10, 1933	6.3	0.612	Subway Terminal, L.A.	59	N39E	3.61	0.0922	A
33	Lower California	Dec. 30, 1934	6.5	1.538	El Centro	58	S00W	7.04	0.0412	B
34	San Fernando California	Feb. 9, 1971	6.4	0.968	2500 Wilshire Blvd., L.A.	40	N61W	5.13	0.0542	B
35	San Fernando California	Feb. 9, 1971	6.4	1.273	3550 Wilshire Blvd., L.A.	39	WEST	6.06	0.0882	B
36	San Fernando California	Feb. 9, 1971	6.4	1.245	222 Figueroa st., L.A.	41	S37W	6.76	0.0622	B
37	San Fernando California	Feb. 9, 1971	6.4	1.098	3470 WilshireBlvd., L.A.	39	S90W	6.21	0.1072	B
38	San Fernando California	Feb. 9, 1971	6.4	1.131	4680 WilshireBlvd., L.A.	38	N15E	5.35	0.0912	B
39	San Fernando California	Feb. 9, 1971	6.4	1.148	445 Figueroa st., L.A.	41	S38W	6.62	0.0692	A
40	San Fernando California	Feb. 9, 1971	6.4	1.018	Hollywood Storage L.A.	32	S00W	6.33	0.0532	B
41	Near E. Coast of Honshu, Japan	May 16, 1968	7.9	2.173	Muroran Harbor	290	N00E	6.67	0.0842	B
42	Near E. Coast of Honshu, Japan	June 17, 1973	7.4	1.971	Kushiro Central Wharf	112	N00E	6.80	0.1662	B
43	Mexico earthquake	Sep. 19, 1985	8.1	0.994	Zihuatenejo, Guerrero Array	135	S00E	6.41	0.0622	A
44	Mexico earthquake	Sep. 19, 1985	8.1	0.501	Teacalco, Cuerrero Array	333	N00E	5.99	0.0272	A
45	Mexico earthquake	Sep. 19, 1985	8.1	0.381	Mesa Vibradora C.U., Mexico City	379	N90W	3.66	0.0362	A

Table 3: Considered near-fault seismic records.

#	Earthquake	Date	Mg	PGA (m/s^2)	Site	Epic. distance (Km)	PGA/PGV (s^{-1})	Specific energy density (m^2/s)	Soil (EC 8 class)
46	Imperial Valley-06	Oct. 15, 1979	6.53	1.763	EC County Center FF	7.31	3.23	0.4562	C
47	Imperial Valley-06	Oct. 15, 1979	6.53	3.708	EC Meloland Overpass FF	0.07	3.23	0.9452	C
48	Imperial Valley-06	Oct. 15, 1979	6.53	3.503	El Centro-Array sta 4	7.05	4.50	0.9552	C
49	Imperial Valley-06	Oct. 15, 1979	6.53	3.683	El Centro-Array sta 5	3.95	4.03	1.2192	C
50	Imperial Valley-06	Oct. 15, 1979	6.53	4.333	El Centro-Array sta 6	1.35	3.88	1.5172	C
51	Imperial Valley-06	Oct. 15, 1979	6.53	4.536	El Centro-Array sta 7	0.56	4.17	1.0322	C
52	Imperial Valley-06	Oct. 15, 1979	6.53	4.591	El Centro-Array sta 8	3.86	9.43	0.4322	C
53	Imperial Valley-06	Oct. 15, 1979	6.53	4.093	El Centro-differential array	5.09	6.85	0.4752	C
54	Morgan Hill	Apr. 24, 1984	6.19	7.985	Coyote Lake Dam (SW Abut)	0.53	12.82	0.1872	B
55	Loma Prieta	Oct. 17, 1989	6.93	2.885	Gilroy. Gavilan Coll.	9.96	9.35	0.0372	B
56	Loma Prieta	Oct. 17, 1989	6.93	9.260	LGPC	3.88	9.52	1.8122	B
57	Landers	June. 28, 1992	7.28	6.911	Lucerne	2.19	5.05	2.1892	B
58	Landers	June. 28, 1992	7.28	2.313	Yermo Fire Station	23.62	4.10	0.6112	C
59	Northridge-01	Jan. 17, 1994	6.69	6.054	Jensen Filter Plant	5.43	6.21	1.0702	B
60	Northridge-01	Jan. 17, 1994	6.69	5.080	Jensen Filter Plant Generator	5.43	7.52	0.7872	B
61	Northridge-01	Jan. 17, 1994	6.69	7.098	Newhall—Fire Station	5.92	5.92	0.8712	C
62	Northridge-01	Jan. 17, 1994	6.69	4.176	Newhall—W Pico Canyon Rd.	5.48	4.76	0.8982	C
63	Northridge-01	Jan. 17, 1994	6.69	8.533	Rinaldi receiving Station	6.5	5.10	1.2272	C
64	Northridge-01	Jan. 17, 1994	6.69	5.830	Sylmar—Converter Station	5.35	4.48	1.9942	C
65	Northridge-01	Jan. 17, 1994	6.69	8.127	Sylmar—Converter Station East	5.19	7.14	0.8242	B
66	Northridge-01	Jan. 17, 1994	6.69	7.187	Sylmar—Olive view Med FF	5.30	5.85	1.0042	B
67	Kobe, Japan	Jan. 17, 1995	6.9	8.380	KJMA	0.96	8.77	1.0032	C
68	Kobe, Japan	Jan. 17, 1995	6.9	6.330	Takarazuka	0.27	8.70	0.3712	C
69	Kocaeli, Turkey	Aug. 17, 1999	7.51	2.367	Gebze	10.92	4.63	0.4682	B
70	Chi-Chi, Taiwan	Sept. 21, 1999	7.62	6.513	CHY028	3.14	8.40	0.5592	B
71	Chi-Chi, Taiwan	Sept. 21, 1999	7.62	3.758	CHY101	9.96	5.00	1.1422	C
72	Chi-Chi, Taiwan	Sept. 21, 1999	7.62	2.808	TCU049	3.78	6.10	0.7612	B
73	Chi-Chi, Taiwan	Sept. 21, 1999	7.62	3.681	TCU052	0.66	2.22	7.2102	B
74	Chi-Chi, Taiwan	Sept. 21, 1999	7.62	2.202	TCU053	5.97	5.38	0.5292	B
75	Chi-Chi, Taiwan	Sept. 21, 1999	7.62	1.538	TCU054	5.30	2.54	0.8612	B
76	Chi-Chi, Taiwan	Sept. 21, 1999	7.62	5.538	TCU068	0.32	3.00	13.8932	B
77	Chi-Chi, Taiwan	Sept. 21, 1999	7.62	3.245	TCU075	0.91	3.66	1.8322	B
78	Chi-Chi, Taiwan	Sept. 21, 1999	7.62	3.045	TCU076	2.76	4.48	0.6212	B
79	Chi-Chi, Taiwan	Sept. 21, 1999	7.62	2.302	TCU082	5.18	3.98	0.9992	B
80	Chi-Chi, Taiwan	Sept. 21, 1999	7.62	1.248	TCU087	7.00	2.86	0.6852	B
81	Chi-Chi, Taiwan	Sept. 21, 1999	7.62	2.083	TCU101	2.13	3.05	0.9102	C
82	Chi-Chi, Taiwan	Sept. 21, 1999	7.62	2.899	TCU102	1.51	2.66	1.9732	B
83	Chi-Chi, Taiwan	Sept. 21, 1999	7.62	1.305	TCU103	6.10	2.10	1.2302	B
84	Chi-Chi, Taiwan	Sept. 21, 1999	7.62	2.195	TCU122	9.35	5.18	0.7462	B
85	Chi-Chi, Taiwan	Sept. 21, 1999	7.62	2.969	WGK	9.96	4.39	0.9892	C

Table 4: Modal analysis data for the considered structural system.

T_y (s)	ε_{kx}	First mode		Second mode	
		Period (s)	Modal component	Period (s)	Modal component
1.0	0.02	$T_1 = 1.002$	$\Phi_{y,1} = 1.000$ $\Phi_{\theta,1} = -0.157$	$T_2 = 0.671$	$\Phi_{y,2} = 0.016$ $\Phi_{\theta,2} = 1.000$
	0.05	$T_1 = 1.012$	$\Phi_{y,1} = 1.000$ $\Phi_{\theta,1} = -0.484$	$T_2 = 0.708$	$\Phi_{y,2} = 0.050$ $\Phi_{\theta,2} = 1.000$
	0.10	$T_1 = 1.070$	$\Phi_{y,1} = -0.790$ $\Phi_{\theta,1} = 1.000$	$T_2 = 0.754$	$\Phi_{y,2} = 0.132$ $\Phi_{\theta,2} = 1.000$

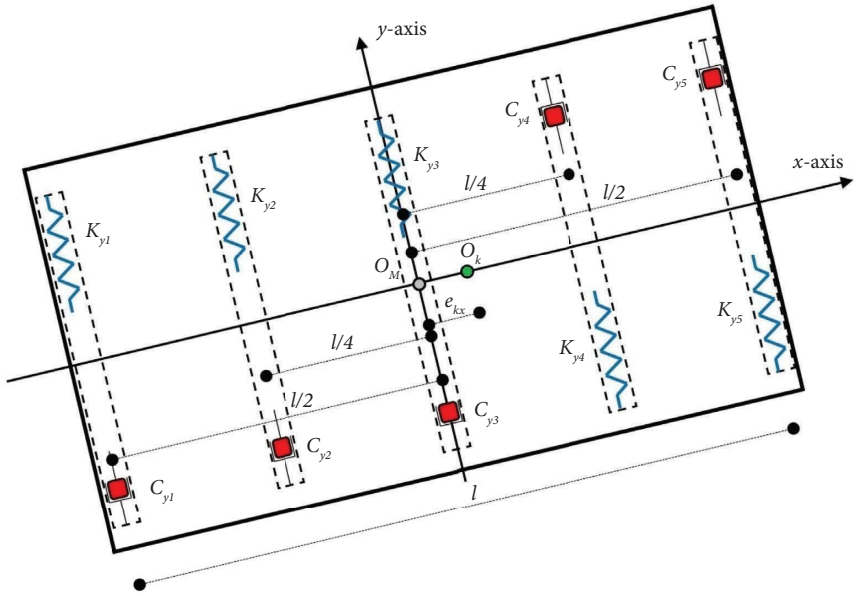

Figure 10: Asymmetric plan-wise system for numerical analysis.

For comparative purposes, in addition to the four control strategies, proposed in this work, the seismic response of asymmetric systems was studied under three other control strategies:

1. No control: all damping and stiffness resources are inactive;
2. Passive control: all damping and stiffness resources are active;
3. KK and/or SH semi-active algorithms: additional stiffness resources are activated based on the Kamagata & Kobori (KK) algorithm [64, 65], whereas extra-structural damping resources follow the Sky–Hook (SH) algorithm [66–68].

Regarding the KK algorithm, it follows the intuitive idea that maximum stiffness is activated when the relative displacement and velocity have the same direction, mimicking human equilibrium process, explained as follows:

$$\begin{cases} dK_i \geq 0 \text{ if } \left(y + \theta x_i\right) \cdot \left(\dot{y} + \dot{\theta} x_i\right) \geq 0, \\ dK_i < 0 \text{ if } \left(y + \theta x_i\right) \cdot \left(\dot{y} + \dot{\theta} x_i\right) < 0, \end{cases} \quad i = 1, 2, \ldots, N, \tag{61}$$

whereas the SH algorithm is designed to emulate the ideal damping value known as the "Sky–Hook damping," in which the linear viscous device generates a force proportional to the absolute velocity of the mass, which is particularly effective in reducing seismic energy transmission from the ground to the structural system. This algorithm is specified by the simple control law of Equation (62):

$$\begin{cases} dC_i \geq 0 \text{ if } \left(y + \theta x_i\right) \cdot \left(\dot{Y} + \dot{\theta} x_i\right) \geq 0, \\ dC_i < 0 \text{ if } \left(y + \theta x_i\right) \cdot \left(\dot{Y} + \dot{\theta} x_i\right) < 0, \end{cases} \quad i = 1, 2, \ldots, N'. \tag{62}$$

These two algorithms were selected for comparison from the various proposals available in the literature because they exhibit a level of complexity and a framework similar to those proposed in this work. In fact, they do not aim to track the optimal action defined by an active control law but rather to tune the semiactively controlled parameters based on the dynamic state of the device.

Figures 11, 12, 13, 14, 15, 16, 17, 18, 19, 20, 21, 22, 23, and 24 present the significant results from the extensive numerical simulations carried out.

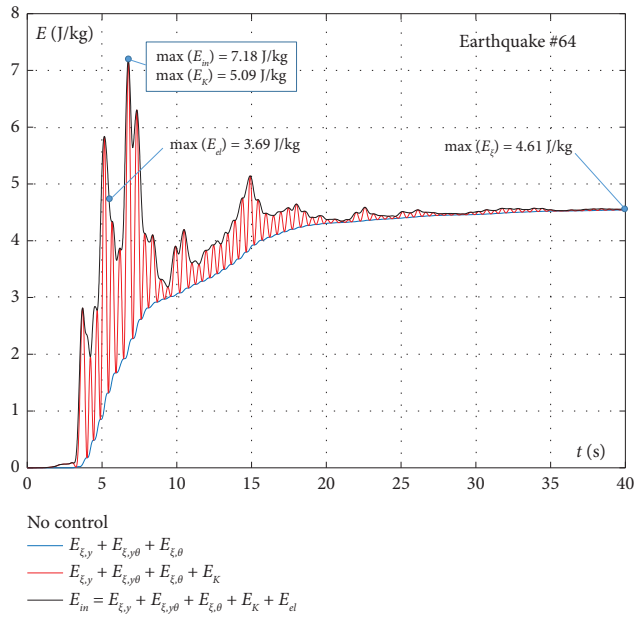

FIGURE 11: No control strategy—asymmetric system: $\varepsilon_{kx} = 0.05$, $T_y = 1.0$ s, $r_K = 0.2$.

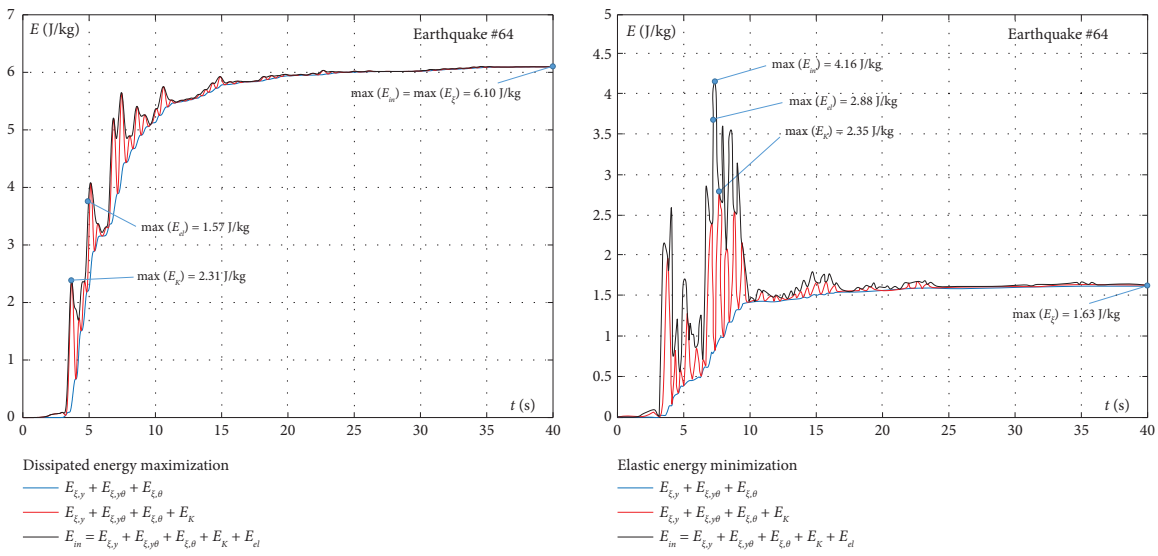

FIGURE 12: Continued.

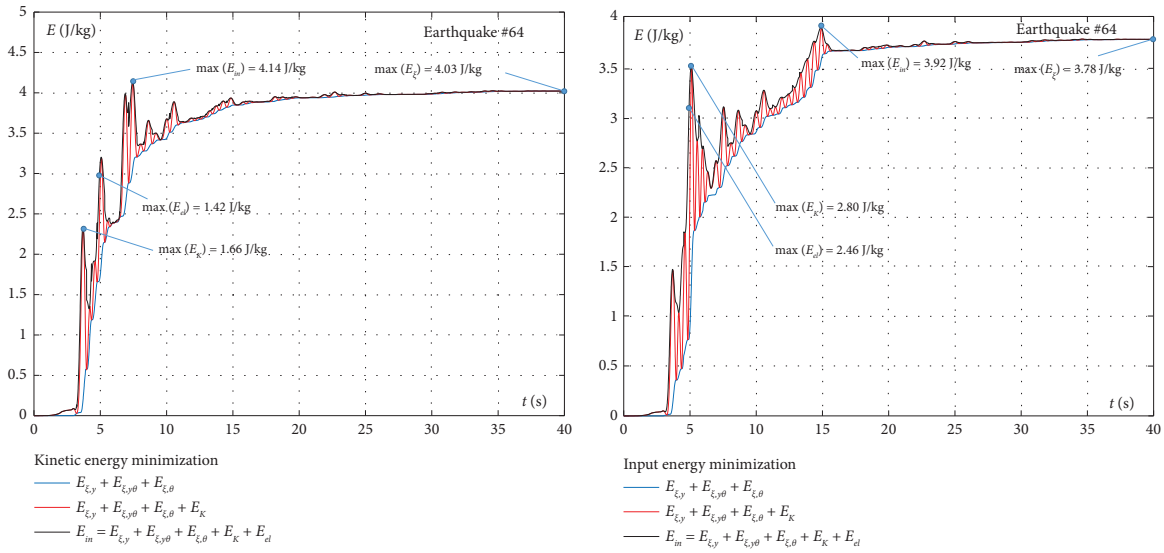

FIGURE 12: Semi-active control strategies—asymmetric system: $\varepsilon_{kx} = 0.05$, $T_y = 1.0$ s, $r_K = 0.2$.

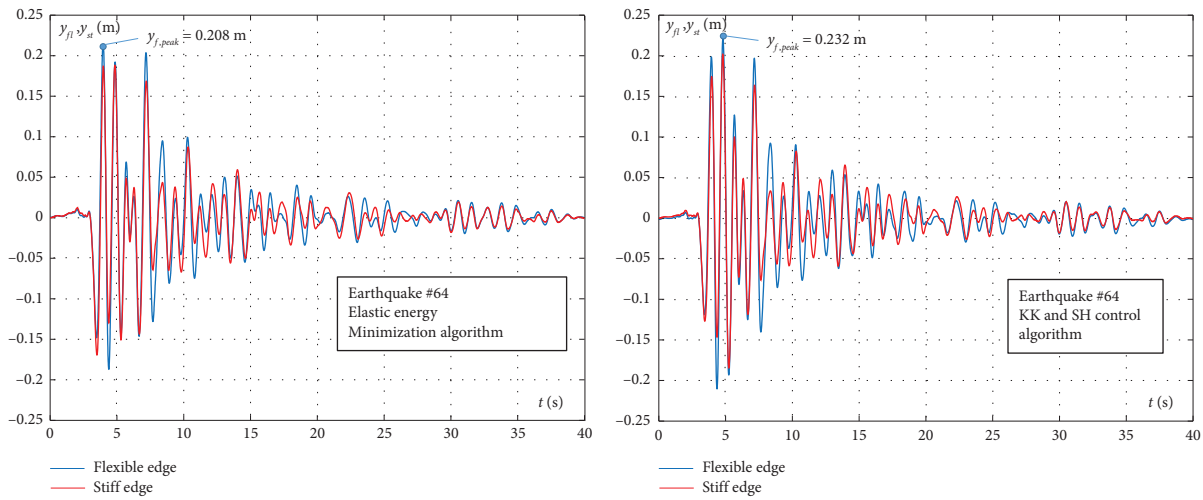

FIGURE 13: Comparison between elastic energy minimization algorithm and KK-SH control algorithms: flexible and stiff edge displacement time-history: $\varepsilon_{kx} = 0.05$, $T_y = 1.0$ sec., $r_k = 0.2$.

Figures 11 and 12 show the time histories of the different energy terms (Equation (10)) with reference to earthquake #64, which is characterized by the highest seismic demand within the considered events. Specifically, Figure 11 presents the case of no control, while Figures 12(a), 12(b), 12(c), and 12(d) show the results when the semi-active devices are regulated according to the four proposed algorithms: maximization of dissipated energy (Figure 12(a)), minimization of elastic energy (Figure 12(b)), minimization of kinetic energy (Figure 12(c)), and minimization of input energy (Figure 12(d)).

Figures 11 and 12 also highlight the maximum values for the four energy rates referred to the different algorithms in the specific represented structural case (i.e., $\varepsilon_{kx} = 0.05$, $T_y = 1.0$ s, $r_K = 0.2$). It is straightforward to verify that, in this specific case, the individual semi-active control algorithms are effective in reducing the respective energy terms compared to both the uncontrolled scenario and those in which an algorithm targeting a different energy objective is considered. When performing this comparison, it should be noted that, in the case of the elastic energy minimization algorithm (Figure 12(b)), the comparison should be carried out with the response of the uncontrolled structure (Figure 11), that is, by considering the same level of available damping.

For this same structural case, Figures 13 and 14, respectively, show displacement and velocity time-histories of both flexible edge, $y_{fl} = y - (1/2)\theta l$, and stiff edge,

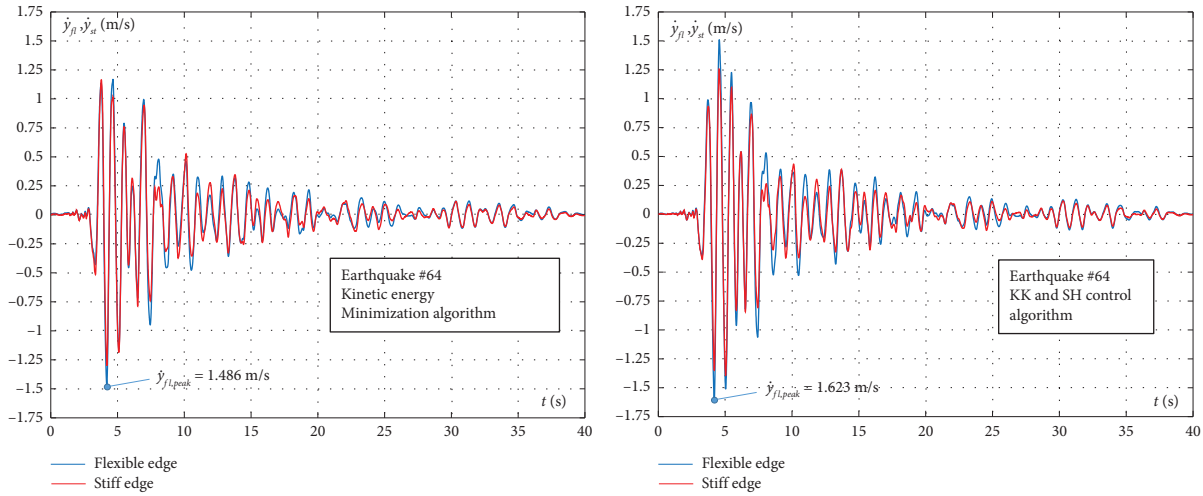

FIGURE 14: Comparison between kinetic energy minimization algorithm and KK-SH control algorithms: flexible and stiff edge displacement time-history: $\varepsilon_{kx} = 0.05$, $T_y = 1.0$ sec., $r_k = 0.2$.

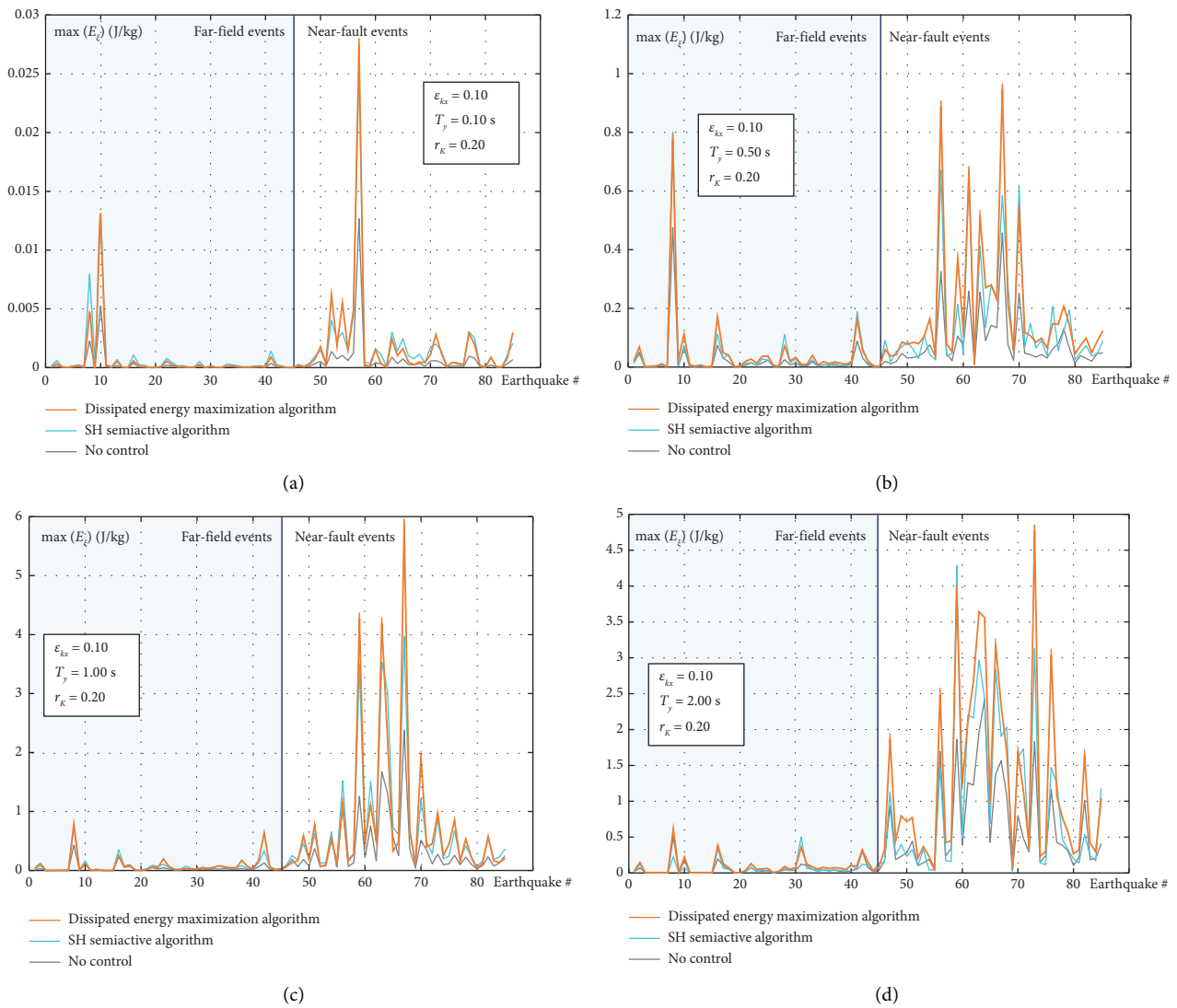

FIGURE 15: Maximum dissipated energy: comparison between different algorithms.

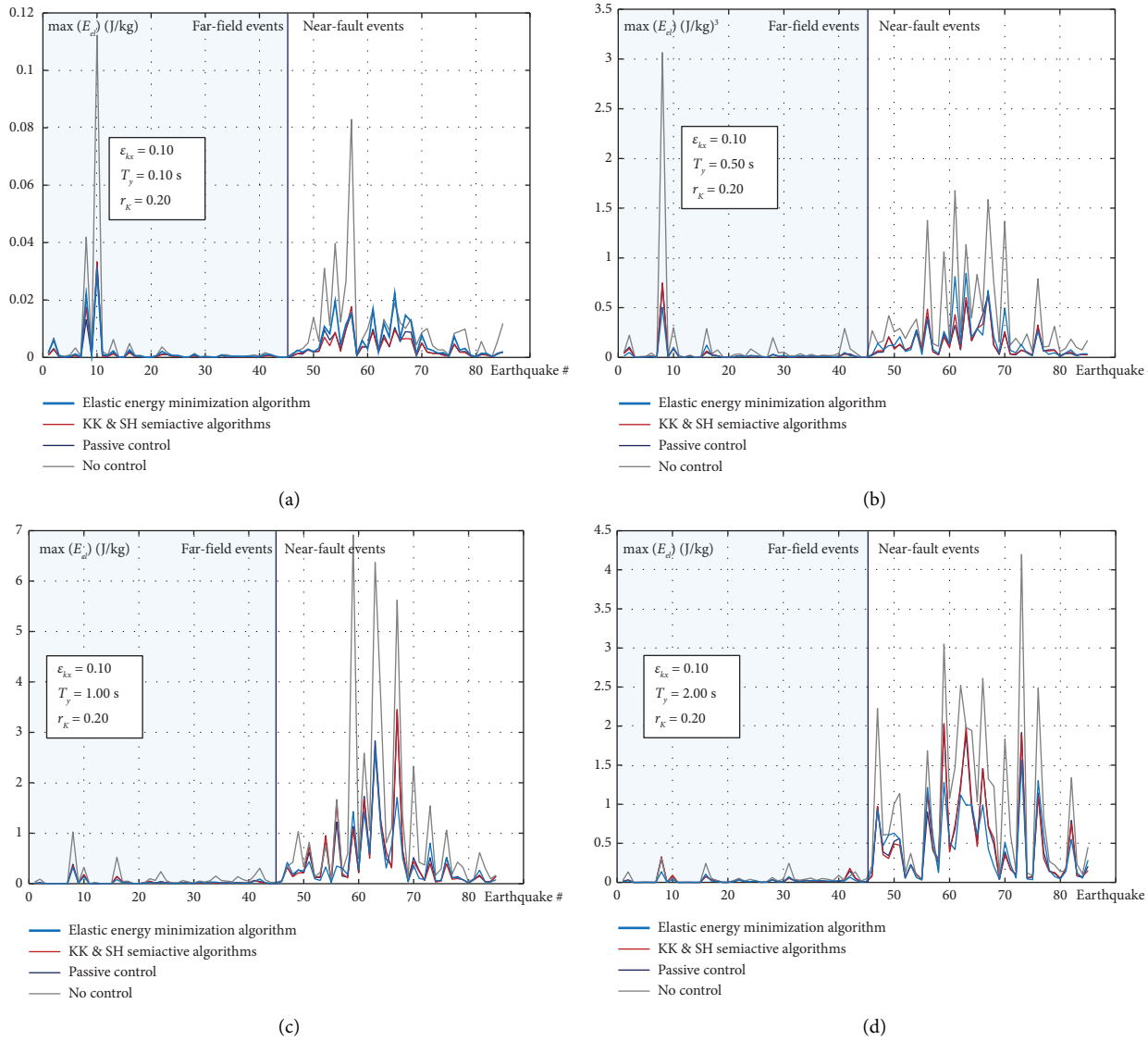

FIGURE 16: Maximum elastic energy: comparison between different algorithms.

$y_{st} = y + (1/2)\theta l$, for the two control algorithms: elastic energy minimization (Figure 13(a)) and kinetic energy minimization (Figure 14(a)) together with their comparison with KK and SH semi-active control algorithms (Figures 13(b) and 14(b)). These figures show a reduction in seismic demand in terms of displacement and velocity, achieved through the proposed algorithms. These results are representative of a general behavior observed in the numerical analyses for near-fault excitations characterized by high seismic demand (as also marked next in Figures 16 and 17).

To extensively test the proposed semi-active control algorithms, a wide parametric analysis was conducted to evaluate the dynamic responses and determine the maximum values of the different energy components for each of the 85 considered seismic records. In detail, for each seismic signal, 300 different asymmetric structural systems were analyzed by varying 5 different values of $r_K = K_y/k_y \in \{0.1, 0.2, 0.3, 0.4, 0.5\}$, 20 values of $T_y = 2\pi/\omega_y$ between 0.1 and 2 sec, and 3 values of the structural eccentricity $\varepsilon_{kx} \in \{0.02, 0.05, 0.10\}$, while applying the different semi-active control strategies (i.e., maximization of dissipated energy, minimization of elastic energy, minimization of kinetic energy, minimization of input energy in addition to no control, passive control, KK, and/or SH semi-active algorithms).

Figures 15, 16, 17, and 18 present, for some relevant cases, the maximum energy rates associated with the semi-active algorithms for each seismic input. Specifically, four cases are illustrated for each algorithm, where practical values for structural eccentricity and available supplemental stiffness are set, and the fundamental vibration period of the asymmetric system is varied from 0.1 sec (rigid structure) to 2 sec (flexible structure).

Figures 15(a), 15(b), 15(c), and 15(d) show a comparison between the maximum values of dissipated energy using the

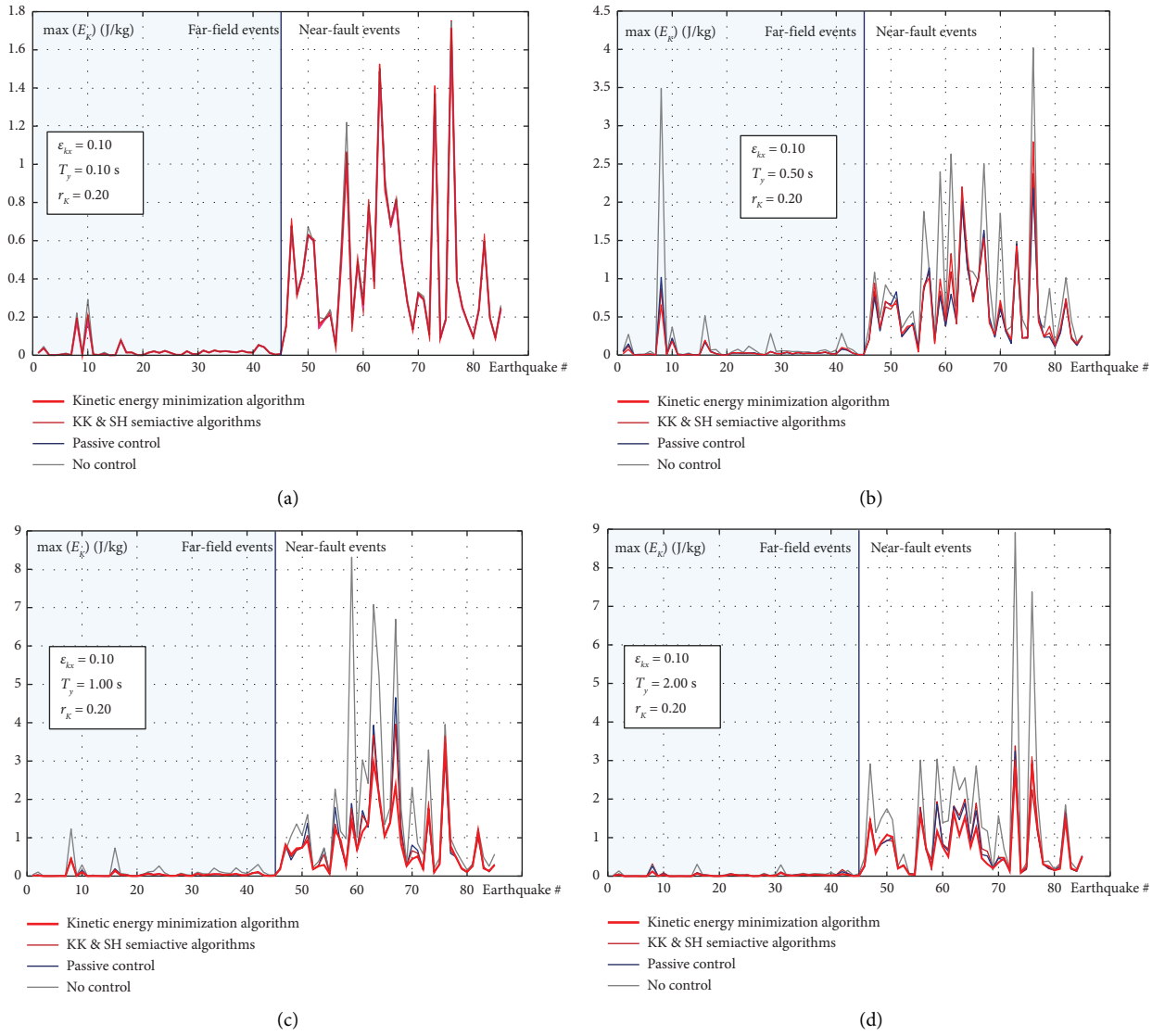

Figure 17: Maximum kinetic energy: comparison between different algorithms.

semi-active control strategy of Equation (16) and the cases with no control action or with the semi-active SH algorithm control. In this particular case, the proposed control strategy aligns with passive control, which, unlike in other cases, is not considered among the alternative strategies. The same comparative analysis is conducted in Figures 16, 17, and 18, respectively, referring to elastic energy, kinetic energy, and input energy. In these cases, since both the stiffness and damping values are modified by the proposed control algorithms, the comparison was made with reference to the KK and SH algorithms.

The results show that for very stiff systems (Figures 15(a) and 18(a)) characterized by a low natural period, the gain obtained through the application of the proposed algorithms is generally limited.

Conversely, for systems having a period greater than 1 sec and, especially, in the case of near-fault events, the reduction in seismic response is significant, although there are specific excitations (e.g., earthquakes #73 and #76) where other strategies lead to comparable results. Figures 15, 16, 17, and 18 highlight how the performance of the proposed control algorithms, in terms of the associated energy components and considering equal available (stiffness and dissipative) extra-structural resources, generally proves to be superior in the case of higher seismic demand. This statement is specifically verified in the case of seismic excitations and asymmetric structures, which correspond to a greater seismic demand. In the case of far-field seismic excitations and stiff asymmetric structures, the application of the proposed algorithms leads to outcomes comparable with those obtained with alternative algorithms.

To summarize the effectiveness of the proposed algorithms, the mean values of different energy rates and peak edge displacements across all seismic excitations, as the translational period T_y of the asymmetric systems varies, are shown in Figures 19, 20, 21, 22, 23, and 24. For each considered energy rate, the corresponding optimization algorithm is compared with an alternative algorithm that uses

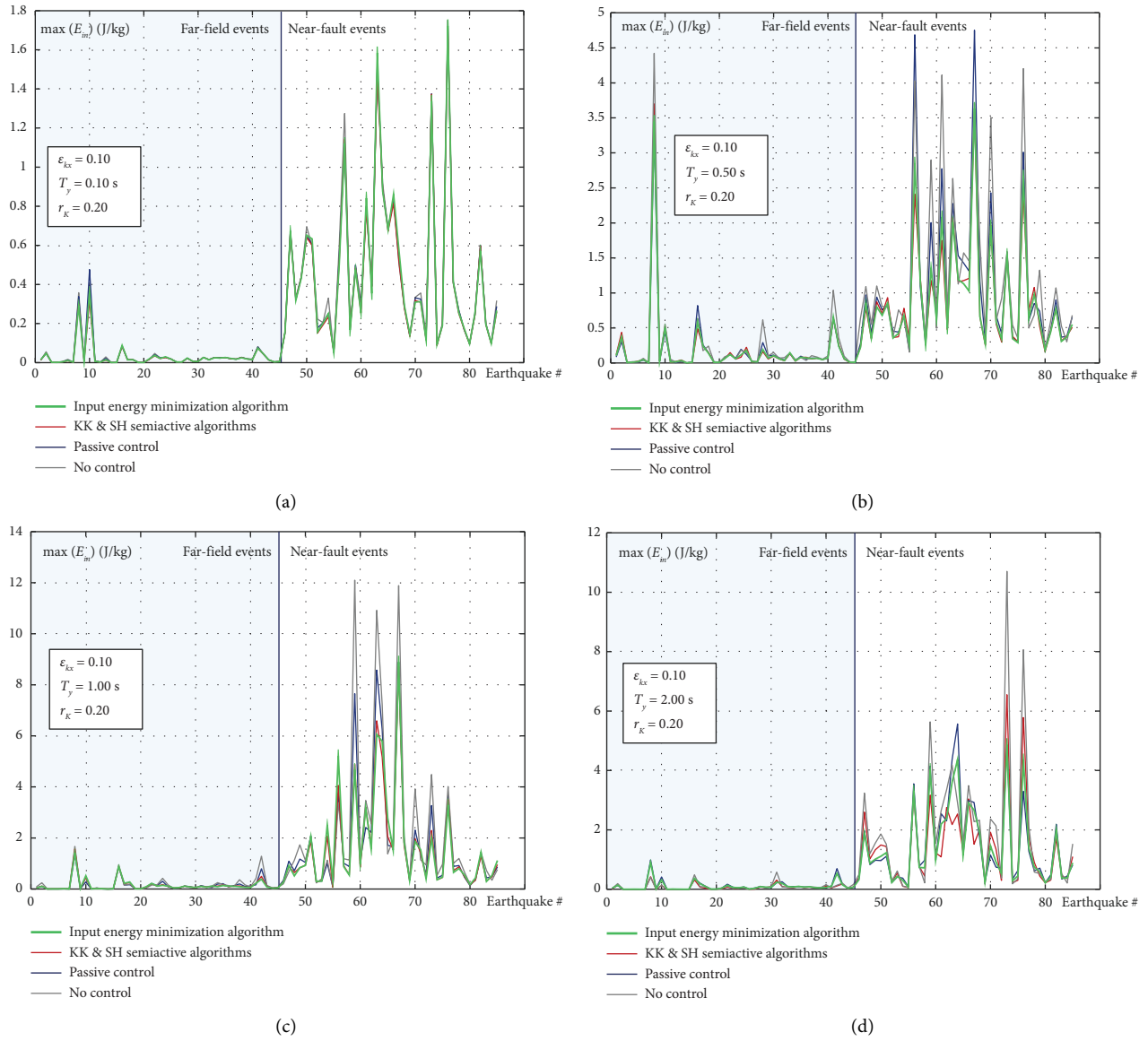

FIGURE 18: Maximum input energy: comparison between different algorithms.

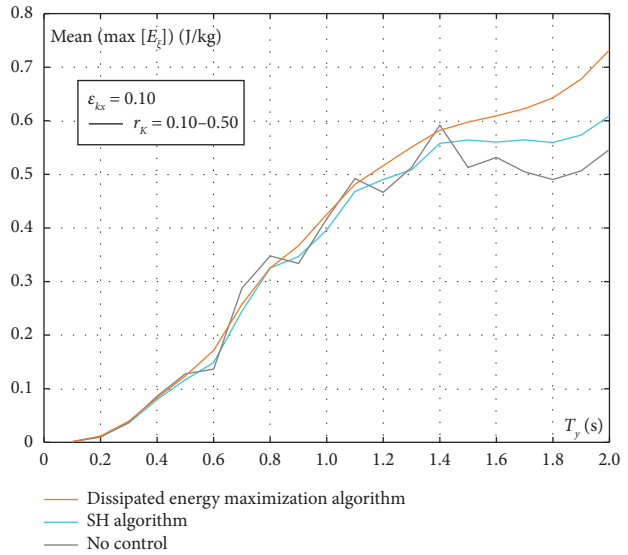

FIGURE 19: Dissipated energy demand averaged over all the seismic events.

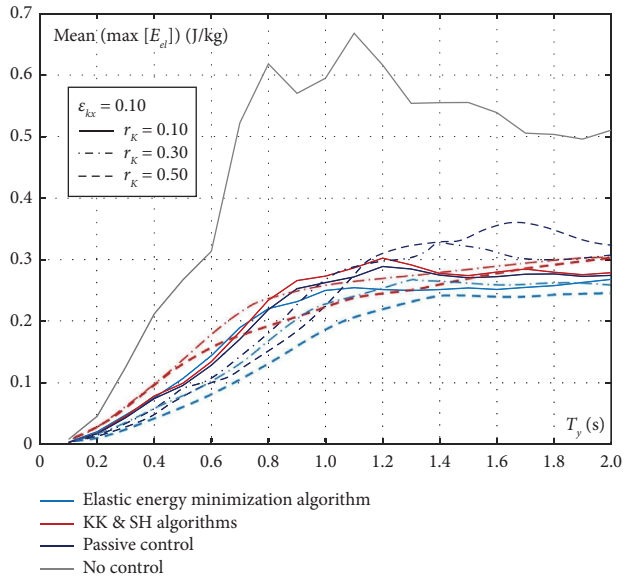

FIGURE 20: Elastic energy demand averaged over all the seismic events.

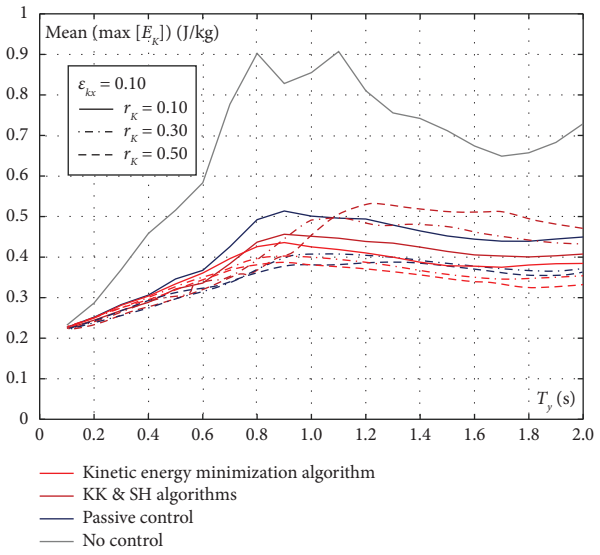

FIGURE 21: Kinetic energy demand averaged over all the seismic events.

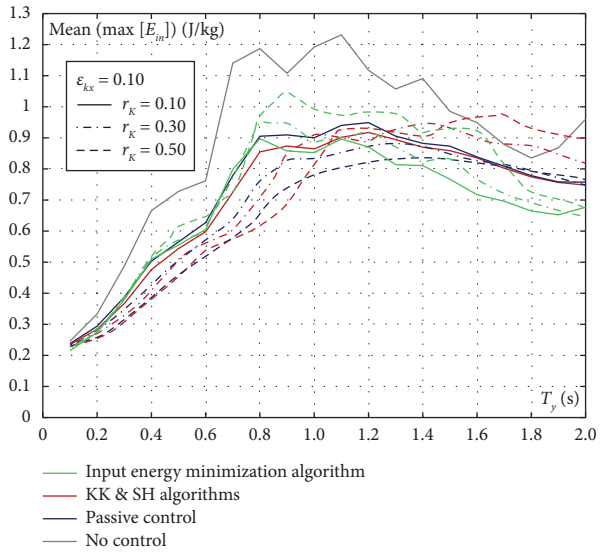

FIGURE 22: Input energy demand averaged over all the seismic events.

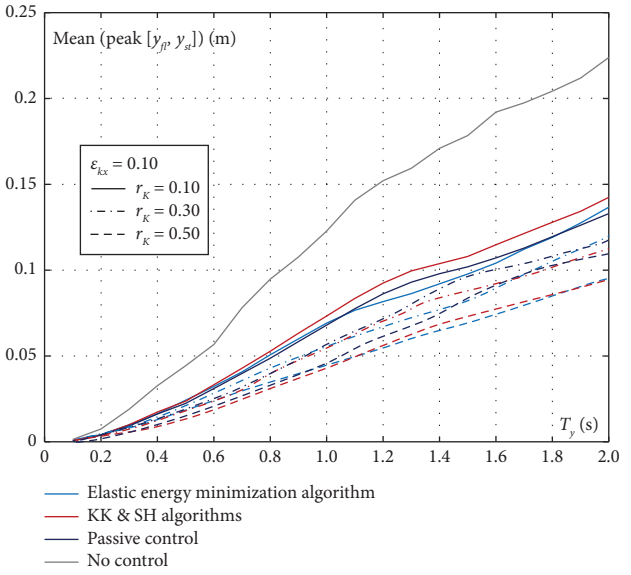

FIGURE 23: Peak edge displacement across all seismic events for the algorithms listed in the legend.

the same amount of supplemental resources for both stiffness and damping, as well as under passive control in addition to the absence of control (Figures 19, 20, 21, and 22). Instead, the elastic energy minimization algorithm has been considered to analyze its effectiveness in controlling the peak edge displacement (Figures 23 and 24). The seismic performances are compared as the available supplemental stiffness resource varies. This choice arises from practical considerations related to the ability to modify the structural stiffness at limited costs. It is also the variable that shows the greatest variations in performance, unlike the considered eccentricity values.

The results obtained highlight the overall effectiveness of the proposed strategies. Specifically, Figure 16 shows how the control algorithm aimed at maximizing the dissipated energy achieves its objective in cases where the seismic demand is higher, namely, for high flexible structural systems. In other cases, its performance is almost identical to that of cases without control or with semi-active control using the SH algorithm. On the other hand, Figure 20 shows how the algorithm aimed at minimizing elastic energy is able to achieve the desired objective across the entire range of natural periods considered for the structural system, especially in cases where the availability of supplemental stiffness

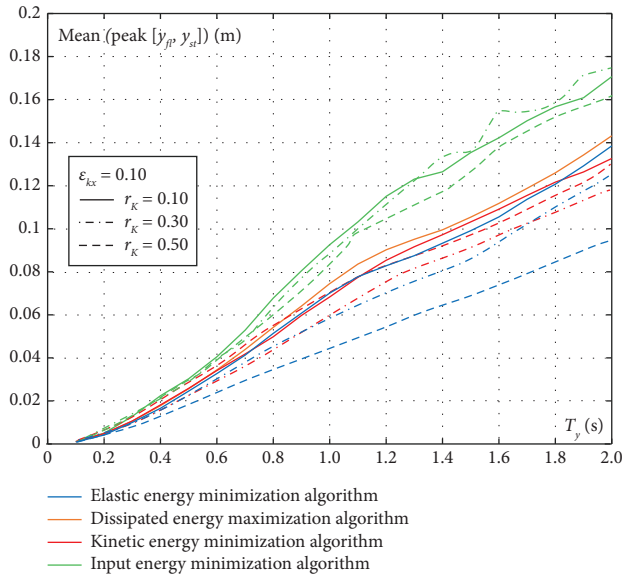

FIGURE 24: Peak edge displacement across all seismic events for the remaining algorithms.

resources increases, even when compared to another semi-active algorithm (i.e., KK semi-active algorithm).

The algorithm based on minimizing kinetic energy also achieves its specific goal but with less pronounced gains and mainly in systems with a natural period greater than 0.8 sec (Figure 21). Before this threshold, its performance is similar to that of simple passive control or a semi-active control of stiffness and damping based on the other tested algorithms (i.e., KK-SH algorithms).

The results are related to input energy shown in Figure 22. As already pointed out in [56] with respect to the semi-active control only of the damping resources, this algorithm shows non-optimal performance in the case of systems having medium–high stiffness. Only in cases where the system has a period greater than 1.5 sec, the input energy, with equal supplemental resources, appears to be effectively minimized compared to the other analyzed cases.

Finally, Figures 23 and 24 show how the elastic energy control algorithm provides good performance in controlling the average seismic demand in terms of displacement across the entire set of considered seismic excitations. In Figure 23, the mean of the peak displacements at the edges of the asymmetric system is shown as the natural vibration period of the structure varies, in the case where the semi-active controller is regulated by the elastic energy minimization algorithm. The figure also presents this quantity for the KK and SH algorithms, passive control, and without control. The results highlight how the proposed algorithm, with the same available supplemental resource, achieves performance aligns with that of passive control in the case of low additional stiffness and with that of the KK and SH algorithms in the case of higher values of r_K. In Figure 24, the same representation is provided for the four algorithms defined in this study to highlight their differences in terms of reducing seismic displacement demand. The numerical analyses demonstrate that, with limited available stiffness resources, the kinetic energy minimization algorithm presents the same effectiveness as the elastic energy algorithm, although this effectiveness decreases significantly when $r_K = 0.5$. In contrast, the algorithm based on input energy minimization proves ineffective in controlling displacements across the entire range of structural systems considered.

5. Conclusions

This study introduces novel semi-active control strategies for managing the dynamic response of plan-wise asymmetric structural systems, with a specific focus on regulating different energy components throughout their dynamic behavior. In contrast to conventional approaches that seek to replicate active control mechanisms, the proposed strategies are grounded in a physically intuitive framework and exploit extra-structural stiffness and damping resources to effectively mitigate seismic demand.

This work presents the following key aspects:

- Four algorithms have been developed and tested, focusing on controlling energy components: maximizing dissipated energy, minimizing elastic energy, minimizing kinetic energy, and minimizing input energy.
- Numerical simulations highlight the effectiveness of the proposed strategies, especially in cases where controlling seismic demand is more critical, such as for flexible structures subjected to near-fault excitations. The results show that these strategies achieve better performance than other semi-active methods of similar complexity.
- A major advantage of the proposed approach is its energy-based formulation, which allows the control algorithm to be tailored to the specific structural problem rather than relying solely on translational motion criteria. This enhances adaptability and effectiveness across different structural configurations and seismic conditions.
- Although displacement demand reduction is not the primary goal of the elastic and kinetic energy minimization algorithms, they prove to be highly effective in limiting peak displacements at the edges. In particular, the elastic energy minimization strategy significantly improves structural performance as the availability of extra-structural stiffness increases.

Some questions have emerged from this study that will be addressed in future research: for certain seismic excitations, the effectiveness of the presented algorithms appears to be reduced. Additionally, this work focuses solely on the linear response of the considered structural systems. Future works can be devoted to extend the proposed strategy to nonlinear cases and to the control of hysteretic energy dissipation, which plays a crucial role in determining damage levels and, consequently, the seismic performance of the structural system.

Data Availability Statement

The data that support the findings of this study are available from the corresponding author upon reasonable request.

Conflicts of Interest

The authors declare no conflicts of interest.

Funding

This study was carried out within the "Data fusion based digital twins for structural safety assessment" project—funded by European Union—Next Generation EU within the PRIN 2022 program (D.D. 104 02/02/2022 Ministero dell'Università e della Ricerca). This manuscript reflects only the authors' views and opinions, and the Ministry cannot be considered responsible for them.

This study was also carried out within the RETURN Extended Partnership and received funding from the European Union—Next Generation EU (National Recovery and Resilience Plan—NRRP, Mission 4, Component 2, Investment 1.3—D.D. 1243 2/8/2022, PE0000005).

This work is also part of the research activity developed by the authors within the framework of the "PNRR": MOST—Sustainable Mobility National Research Center—SPOKE 7 "Cooperative Connected and Automated Mobility and Smart Infrastructures"—WP4 and received funding from the European Union Next-GenerationEU (PIANO NAZIONALE DI RIPRESA E RESILIENZA (PNRR)—MISSIONE 4 COMPONENTE 2, INVESTIMENTO 1.4—D.D. 1033 17/06/2022).

References

[1] M. R. Mansoori and A. S. Moghadam, "Using Viscous Damper Distribution to Reduce Multiple Seismic Responses of Asymmetric Structures," *Journal of Constructional Steel Research* 65, no. 12 (2009): 2176–2185, https://doi.org/10.1016/j.jcsr.2009.06.016.

[2] Z. Alam, L. Sun, C. Zhang, Z. Su, and B. Samali, "Experimental and Numerical Investigation on the Complex Behaviour of the Localised Seismic Response in a Multi-Storey Plan-Asymmetric Structure," *Structure and infrastructure engineering* 17, no. 1 (2021): 86–102, https://doi.org/10.1080/15732479.2020.1730914.

[3] L. Esteva, "Earthquake Engineering Research and Practice in Mexico after the 1985 Earthquakes," *Bulletin of the New Zealand Society for Earthquake Engineering* 20, no. 3 (1987): 159–200, https://doi.org/10.5459/bnzsee.20.3.159-200.

[4] O. Yoshida and S. J. Dyke, "Response Control of Full-Scale Irregular Buildings Using Magnetorheological Dampers," *Journal of Structural Engineering* 131, no. 5 (2005): 734–742, https://doi.org/10.1061/(asce)0733-9445(2005)131:5(734).

[5] M. Ozturk, M. H. Arslan, and H. H. Korkmaz, "Effect on RC Buildings of 6 February 2023 Turkey Earthquake Doublets and New Doctrines for Seismic Design," *Engineering Failure Analysis* 153 (2023): 107521, https://doi.org/10.1016/j.engfailanal.2023.107521.

[6] D. M. Siringoringo and Y. Fujino, "Seismic Response Analyses of an Asymmetric Base-isolated Building during the 2011 Great East Japan (Tohoku) Earthquake," *Structural Control and Health Monitoring* 22, no. 1 (2015): 71–90, https://doi.org/10.1002/stc.1661.

[7] C. Zhang, Z. Alam, L. Sun, and B. Samali, *Seismic Performance of Asymmetric Building Structures* (CRC Press, 2020).

[8] A. K. Chopra and R. K. Goel, "Evaluation of Torsional Provisions in Seismic Codes," *Journal of Structural Engineering* 117, no. 12 (1991): 3762–3782, https://doi.org/10.1061/(asce)0733-9445(1991)117:12(3762).

[9] A. Ghersi and P. P. Rossi, "Influence of Bi-directional Ground Motions on the Inelastic Response of One-Storey In-Plan Irregular Systems," *Engineering Structures* 23, no. 6 (2001): 579–591, https://doi.org/10.1016/s0141-0296(00)00088-2.

[10] T. Paulay, "Some Design Principles Relevant to Torsional Phenomena in Ductile Buildings," *Journal of Earthquake Engineering* 5, no. 3 (2001): 273–308, https://doi.org/10.1080/13632460109350395.

[11] A. J. Kosmopoulos and M. N. Fardis, "Simple Models for Inelastic Seismic Analysis of Asymmetric Multistory RC Buildings," *Journal of Earthquake Engineering* 12, no. 5 (2008): 704–727, https://doi.org/10.1080/13632460701673126.

[12] A. Lucchini, G. Monti, and S. Kunnath, "Nonlinear Response of Two-Way Asymmetric Single-Story Building under Biaxial Excitation," *Journal of Structural Engineering* 137, no. 1 (2011): 34–40, https://doi.org/10.1061/(asce)st.1943-541x.0000266.

[13] R. Tabatabaei and H. Saffari, "Evaluation of the Torsional Response of Multistory Buildings Using Equivalent Static Eccentricity," *Journal of Structural Engineering* 137, no. 8 (2011): 862–868, https://doi.org/10.1061/(asce)st.1943-541x.0000324.

[14] D. Basu, M. C. Constantinou, and A. S. Whittaker, "An Equivalent Accidental Eccentricity to Account for the Effects of Torsional Ground Motion on Structures," *Engineering Structures* 69 (2014): 1–11, https://doi.org/10.1016/j.engstruct.2014.02.038.

[15] S. E. Abdel Raheem, M. M. Ahmed, M. M. Ahmed, and A. G. Abdel-shafy, "Evaluation of Plan Configuration Irregularity Effects on Seismic Response Demands of L-Shaped MRF Buildings," *Bulletin of Earthquake Engineering* 16, no. 9 (2018): 3845–3869, https://doi.org/10.1007/s10518-018-0319-7.

[16] C. G. Stathi, N. P. Bakas, N. D. Lagaros, and M. Papadrakakis, "Ratio of Torsion (ROT): An Index for Assessing the Global Induced Torsion in Plan Irregular Buildings," *Earthquakes and Structures* 9, no. 1 (2015): 145–171, https://doi.org/10.12989/eas.2015.9.1.145.

[17] E. Yaghoubi, A. R. Emami, and M. S. Birzhandi, "IDA-based Collapse Safety Assessment of Torsional-Irregular Buildings, Considering Ductility and Damage," *International Journal of Structural Stability and Dynamics* 23, no. 20 (2023): https://doi.org/10.1142/s0219455423502000.

[18] M. Garcia, J. C. de la Llera, and J. L. Almazán, "Torsional Balance of Plan Asymmetric Structures with Viscoelastic Dampers," *Engineering Structures* 29, no. 6 (2007): 914–932, https://doi.org/10.1016/j.engstruct.2006.06.022.

[19] L. Petti and M. De Iuliis, "Torsional Seismic Response Control of Asymmetric-Plan Systems by Using Viscous Dampers," *Engineering Structures* 30, no. 11 (2008): 3377–3388, https://doi.org/10.1016/j.engstruct.2008.05.023.

[20] P. Castaldo and M. De Iuliis, "Optimal Integrated Seismic Design of Structural and Viscoelastic Bracing-damper Systems," *Earthquake Engineering & Structural Dynamics* 43, no. 12 (2014): 1809–1827, https://doi.org/10.1002/eqe.2425.

[21] Z. Alam, C. Zhang, and B. Samali, "The Role of Viscoelastic Damping on Retrofitting Seismic Performance of Asymmetric Reinforced Concrete Structures," *Earthquake Engineering and Engineering Vibration* 19, no. 1 (2020): 223–237, https://doi.org/10.1007/s11803-020-0558-x.

[22] R. Milanchian and M. Hosseini, "Torsional Response Reduction of Plan-Asymmetric Vertical Seismic Isolation by Appropriate Distribution of Viscous and Viscoelastic

Dampers," *Structures* 27 (October 2020): 962–974, https://doi.org/10.1016/j.istruc.2020.07.009.

[23] J. L. Lin, T. H. Liu, and K. C. Tsai, "Real-valued Modal Response History Analysis for Asymmetric-Plan Buildings with Nonlinear Viscous Dampers," *Soil Dynamics and Earthquake Engineering* 77 (2015): 97–110, https://doi.org/10.1016/j.soildyn.2015.05.002.

[24] J. C. De la Llera, J. L. Almazán, and I. J. Vial, "Torsional Balance of Plan-asymmetric Structures with Frictional Dampers: Analytical Results," *Earthquake Engineering & Structural Dynamics* 34, no. 9 (2005): 1089–1108, https://doi.org/10.1002/eqe.469.

[25] J. Kim and J. Jeong, "Seismic Retrofit of Asymmetric Structures Using Steel Plate Slit Dampers," *Journal of Constructional Steel Research* 120 (2016): 232–244, https://doi.org/10.1016/j.jcsr.2016.02.001.

[26] S. V. Bakre, R. S. Jangid, and G. R. Reddy, "Optimum X-Plate Dampers for Seismic Response Control of Piping Systems," *International Journal of Pressure Vessels and Piping* 83, no. 9 (2006): 672–685, https://doi.org/10.1016/j.ijpvp.2006.05.003.

[27] G. Sawai and S. Dongawar, "Seismic Performance of RC Building with X-Plate and Accordion Metallic Dampers," *International Journal of Innovative Research in Technology* 8, no. Issue 12 (2022).

[28] G. Espinoza, E. Casanova, F. Benedetti, R. Mena, and J. L. Almazán, "Optimal TMD Design for Torsional Balance of Asymmetrical 3D Structures Considering Soil–Structure Interaction," *Structural Control and Health Monitoring* 29, no. 1 (2022): e2858, https://doi.org/10.1002/stc.2858.

[29] G. Espinoza, J. L. Almazán, F. Benedetti, and C. Jara, "Torsional Balance of Nonlinear Asymmetrical Structures by Means of a Tuned Mass Damper," *Structural Control and Health Monitoring* 26, no. 11 (2019): e2442, https://doi.org/10.1002/stc.2442.

[30] N. B. Desu, S. K. Deb, and A. Dutta, "Coupled Tuned Mass Dampers for Control of Coupled Vibrations in Asymmetric Buildings," *Structural Control and Health Monitoring* 13, no. 5 (2006): 897–916, https://doi.org/10.1002/stc.64.

[31] L. Huo and H. Li, "Torsionally Coupled Response Control of Structures," in *13th World Conf. Earthq. Eng. Conf. Proceedings, Vancouver, Br*, 13 (Columbia, Canada, August 2004).

[32] C. Li and X. Gu, "Design of Fluid Viscous Dampers for Single-Story Asymmetric-Plan Buildings Based on LQR Theory," *2010 Second International Conference on Computer Modeling and Simulation* 1 (2010): 49–53, https://doi.org/10.1109/iccms.2010.70.

[33] C. Fu, "Transforming Method of TLCD-Structure to TMD-Structure for Vibration Control," *KSCE Journal of Civil Engineering* 22, no. 4 (2018): 1384–1393, https://doi.org/10.1007/s12205-017-0287-5.

[34] L. Wang, Y. Zhou, S. Nagarajaiah, and W. Shi, "Bi-directional Semi-active Tuned Mass Damper for Torsional Asymmetric Structural Seismic Response Control," *Engineering Structures* 294 (2023): 116744, https://doi.org/10.1016/j.engstruct.2023.116744.

[35] A. Y. Pisal and R. S. Jangid, "Dynamic Response of Structure with Tuned Mass Friction Damper," *International Journal of Advanced Structural Engineering* 8, no. 4 (2016): 363–377, https://doi.org/10.1007/s40091-016-0136-7.

[36] T. Sano, K. Shirai, O. Yoshida, and T. Nishikage, "Assessment of a Seismic Tuned Mass Damper with Friction Fail-Safe Mechanism for the Vibration Control of High-Rise Buildings," *Structural Control and Health Monitoring* 28, no. 12 (2021): e2831, https://doi.org/10.1002/stc.2831.

[37] S. Etedali, M. Akbari, and M. Seifi, "Friction Tuned Mass Dampers in Seismic-Excited High-Rise Buildings with SSI Effects: A Reliability Assessment," *Journal of Earthquake and Tsunami* 17, no. 02 (2023): 2250022, https://doi.org/10.1142/s1793431122500221.

[38] C. Sun and S. Nagarajaiah, "Study on Semi-active Tuned Mass Damper with Variable Damping and Stiffness under Seismic Excitations," *Structural Control and Health Monitoring* 21, no. 6 (2013): 890–906, https://doi.org/10.1002/stc.1620.

[39] L. Wang, W. Shi, X. Li, Q. Zhang, and Y. Zhou, "An Adaptive-Passive Retuning Device for a Pendulum Tuned Mass Damper Considering Mass Uncertainty and Optimum Frequency," *Structural Control and Health Monitoring* 26, no. 7 (2019): e2377, https://doi.org/10.1002/stc.2377.

[40] L. Wang, S. Nagarajaiah, W. Shi, and Y. Zhou, "Seismic Performance Improvement of Base-Isolated Structures Using a Semi-active Tuned Mass Damper," *Engineering Structures* 271 (2022): 114963, https://doi.org/10.1016/j.engstruct.2022.114963.

[41] K. Karami and H. Ahmadi, "Torsional Control of Asymmetric Buildings Using Online 3-D Damage Detection and Adaptive Stiffness Devices," *Structural Control and Health Monitoring* 28, no. 10 (2021): e2804, https://doi.org/10.1002/stc.2804.

[42] H. N. Li and X. L. Li, "Experiment and Analysis of Torsional Seismic Responses for Asymmetric Structures with Semi-active Control by MR Dampers," *Smart Materials and Structures* 18, no. 7 (2009): 075007, https://doi.org/10.1088/0964-1726/18/7/075007.

[43] M. Braz-César and R. Barros, "Optimal Control of a Plan Asymmetric Structure Using Magnetorheological Dampers," *Archive of Applied Mechanics* 87, no. 5 (2017): 893–904, https://doi.org/10.1007/s00419-016-1191-z.

[44] M. T. Braz-César, P. L. Folhento, and R. C. Barros, "Numerical Simulation of Torsional Response Control of a Plan-Eccentric Mass Distribution Building by Using Magnetorheological Dampers," in *2018 13th APCA International Conference on Automatic Control and Soft Computing (CONTROLO)* (IEEE, June 2018), 358–363.

[45] S. M. Zahrai and H. Salehi, "Semi-active Seismic Control of Mid-rise Structures Using Magneto-Rheological Dampers and Two Proposed Improving Mechanisms," *Iranian Journal of Science and Technology. Transactions of Civil Engineering* 38, no. C1 (2014): 21.

[46] S. Panchanan, P. Kumar, S. Basu, and R. S. Jangid, "Seismic Response of Asymmetric Structure with Soil Structure Interaction Using Semi-active MR Damper," in *Recent Advances in Computational Mechanics and Simulations: Volume-I: Materials to Structures* (Singapore: Springer, 2021), 457–468.

[47] A. Bahar, F. Pozo, M. R. Meybodi, and S. Karami, "Magnetorheological Fluid Dampers: A Close Look at Efficient Parametric Models," *Structural Control and Health Monitoring* 2024, no. 1 (2024): 6860185, https://doi.org/10.1155/2024/6860185.

[48] N. H. McClamroch and H. P. Gavin, "Closed Loop Structural Control Using Electrorheological Dampers," in *Proceedings of 1995 American Control Conference-Acc'95*, 6 (IEEE, June 1995), 4173–4177, https://doi.org/10.1109/acc.1995.532717.

[49] S. J. Dyke, B. F. Spencer, M. K. Sain, and J. D. Carlson, "Modeling and Control of Magnetorheological Dampers for Seismic Response Reduction," *Smart Materials and Structures* 5, no. 5 (1996): 565–575, https://doi.org/10.1088/0964-1726/5/5/006.

[50] F. Sadek and B. Mohraz, "Semiactive Control Algorithms for Structures with Variable Dampers," *Journal of Engineering*

Mechanics 124, no. 9 (1998): 981–990, https://doi.org/10.1061/(asce)0733-9399(1998)124:9(981).

[51] N. G. Pnevmatikos and G. D. Hatzigeorgiou, "Seismic Response of Active or Semi Active Control for Irregular Buildings Based on Eigenvalues Modification," *Earthquakes and Structures* 6, no. 6 (2014): 647–664, https://doi.org/10.12989/eas.2014.6.6.647.

[52] M. Sever, H. Yazici, G. Goktas, and I. B. Kucukdemiral, "Disturbance Attenuation of Asymmetric Structure by LMI Based Optimal State Feedback Controller with Saturated Actuators," in *2015 6th International Conference on Modeling, Simulation, and Applied Optimization (ICMSAO)* (IEEE, May 2015), 1–6.

[53] R. K. Goel, "Seismic Response of Asymmetric Systems: Energy-Based Approach," *Journal of Structural Engineering* 123, no. 11 (1997): 1444–1453, https://doi.org/10.1061/(asce)0733-9445(1997)123:11(1444).

[54] A. Yanik, U. Aldemir, and M. Bakioglu, "Energy-based Evaluation of Seismic Response of Structures with Passive and Active Systems," *Proc. of the Earthquake Resistant Engineering Structures* 8 (2011): 67–78.

[55] D. H. Zelleke and V. A. Matsagar, "Semi-active Algorithm for Energy-based Predictive Structural Control Using Tuned Mass Dampers," *Computer-Aided Civil and Infrastructure Engineering* 34, no. 11 (2019): 1010–1025, https://doi.org/10.1111/mice.12474.

[56] M. De Iuliis and P. Castaldo, "An Energy-Based Approach to the Seismic Control of One-Way Asymmetrical Structural Systems Using Semi-active Devices," *Ingegneria Sismica* 29, no. 4 (2012): 31–50.

[57] M. Ismail, "Elimination of Torsion and Pounding of Isolated Asymmetric Structures under Near-fault Ground Motions," *Structural Control and Health Monitoring* 22, no. 11 (2015): 1295–1324, https://doi.org/10.1002/stc.1746.

[58] K. Walsh, M. Abdullah, and C. A. Moore, "Control of Civil Structures Using a Semiactive Stiffness System Based on Variable Amplification," *Journal of Structural Engineering* 134, no. 7 (2008): 1246–1251, https://doi.org/10.1061/(asce)0733-9445(2008)134:7(1246).

[59] S. Nagarajaiah and S. Sahasrabudhe, "Seismic Response Control of Smart Sliding Isolated Buildings Using Variable Stiffness Systems: an Experimental and Numerical Study," *Earthquake Engineering & Structural Dynamics* 35, no. 2 (2005): 177–197, https://doi.org/10.1002/eqe.514.

[60] Z. W. Xing, M. Yu, J. Fu, Y. Wang, and L. J. Zhao, "A Laminated Magnetorheological Elastomer Bearing Prototype for Seismic Mitigation of Bridge Superstructures," *Journal of Intelligent Material Systems and Structures* 26, no. 14 (2015): 1818–1825, https://doi.org/10.1177/1045389x15577654.

[61] Y. Hwang, J. Lee, S. Kye, and H.-J. Jung, "Development of Multi-Layered Electromagnetic System for Improving Base Isolator Using a Magnetorheological Elastomer," *Smart Materials and Structures* 29, no. 11 (2020): 114002, https://doi.org/10.1088/1361-665x/aba9aa.

[62] M. De Iuliis, E. Miceli, and P. Castaldo, "Machine Learning Modelling of Structural Response for Different Seismic Signal Characteristics: A Parametric Analysis," *Applied Soft Computing* 164 (2024): 112026, https://doi.org/10.1016/j.asoc.2024.112026.

[63] P. Castaldo and E. Miceli, "Optimal Single Concave Sliding Device Properties for Isolated Multi-Span Continuous Deck Bridges Depending on the Ground Motion Characteristics," *Soil Dynamics and Earthquake Engineering* 173 (2023): 108128, https://doi.org/10.1016/j.soildyn.2023.108128.

[64] T. Kobori, "Active Variable Stiffness System-Active Seismic Response Control," *Proc. US-Italy-Japan Workshop/Symposium on Structural Control and Intelligent Systems* 1992 (1992): 140–153.

[65] S. Kamagata, "Autonomous Adaptive Control of Active Variable Stiffness System for Seismic Ground Motion," *Proceedings of the First World Conference on Structural Control* 2 (1994): TA4–33.

[66] D. Karnopp, M. J. Crosby, and R. A. Harwood, "Vibration Control Using Semi-active Force Generators," *Journal of Engineering for Industry* 96, no. 2 (1974): 619–626, https://doi.org/10.1115/1.3438373.

[67] D. Karnopp, "Design Principles for Vibration Control Systems Using Semi-active Dampers," *Journal of Dynamic Systems, Measurement, and Control* 112, no. 3 (1990): 448–455, https://doi.org/10.1115/1.2896163.

[68] M. Ahmadian, "On the Isolation Properties of Semiactive Dampers," *Journal of Vibration and Control* 5, no. 2 (1999): 217–232, https://doi.org/10.1177/107754639900500204.